Particle Image Velocimetry of Suspension Plasma Spray in the Vicinity of a Substrate

Sadaf Mohammadi

A Thesis
in
The Department
of
Mechanical, Industrial and Aerospace Engineering (MIAE)

Presented in Partial Fulfillment of the Requirements
for the Degree of
Master of Applied Science (Mechanical Engineering) at
Concordia University
Montréal, Québec, Canada

December 2020

CONCORDIA UNIVERSITY
School of Graduate Studies

This is to certify that the thesis prepared

By: **Sadaf Mohammadi**
Entitled: **Particle Image Velocimetry of Suspension Plasma Spray in the Vicinity of a Substrate**

and submitted in partial fulfillment of the requirements for the degree of

Master of Applied Science (Mechanical Engineering)

complies with the regulations of this University and meets the accepted standards with respect to originality and quality.
Signed by the Final Examining Committee:

_____ Chair
Dr. Lyes Kadem

_____ External Examiner
Dr. Samuel Li

_____ Examiner
Dr. Lyes Kadem

_____ Supervisor
Dr. Christian Moreau and Ali Dolatabadi

Approved by _____
-, Chair
Department of Mechanical, Industrial and Aerospace Engineering (MIAE)

December 14, 2020

_____
Mourad Debbabi, Dean
Faculty of Engineering and Computer Science

Abstract

Particle Image Velocimetry of Suspension Plasma Spray in the Vicinity of a Substrate

Sadaf Mohammadi

Thermal spray technology is a widely used technique in the industry in which surfaces of components are coated by spraying a wide range of metals or ceramics. Considering the growing interest in building nanostructured coatings due to their unique characteristics, a new technique called suspension plasma spraying is developed. Suspension plasma spraying (SPS) is one of the promising methods that can be used to achieve coatings with fine microstructure and superior properties. Several significant parameters make this SPS process complex to understand and control. In particular, the velocity and diameter of in-flight particles near the substrate, which depend on the plasma and injection conditions, have a strong influence on the coating columnar structure. In this work, the velocity of in-flight particles in the vicinity of the substrate and free jet was investigated by the particle image velocimetry (PIV) method. This study is aimed at providing a better understanding of the behavior of in-flight particles in the SPS process. A suspension of titania particles is used here taking advantage to the abundance and chemical stability of titania and its use in different SPS applications. Observations and results of this work showed that the trajectory and velocity of micron-size particles, due to their small Stokes number, are strongly influenced by the presence of the substrate. The PIV results make it possible to visualize the suspension injection into the plasma with titania aqueous suspension. Particle velocity reported by PIV method corresponded likely to un-molten particles in SPS process. The PIV measurements were finally compared with velocity measurements carried out with a thermal-emission particle sensor in the same spray condition as the PIV run.

Acknowledgments

Hereby I would like to express my sincere gratitude and appreciation to Professor Ali Dolatabadi and Professor Christian Moreau for their continuous help and support without which this research would not have been possible. Their dedication and patience have led me through this journey from the very be- ginning to the end. Also, I would like to appreciate their continuous guidance, patience, encouragement, and support during these years of my study. I wish to thank the Concordia University Thermal Spray Laboratory group members for all the help and encouragement during my work. Special thanks to Dr. Fadhel Ben Ettouil and Dr. Ali Akbarnozari for all the technical assistance during my experimental work. I would also like to appreciate Hediyeh Khatibnezhad and Maryam Zebarjad for their support during these challenging periods. Thank you for being such a great and helpful team.

Last but not least, all my gratefulness to my parents, Zohreh Daeipour and Bahram Mohammadi, without their unconditional love and support, my master studies would not have been possible; thank you for your continuous encouragement to pursue my dreams and always believing in me.

Contents

List of Figures

List of Tables

Acronyms

SPS	Suspension plasma spray
APS	Atmospheric plasma spray
HVOF	High velocity oxygen fuel
TES	Thermal emission sensors
EB-PVD	Electron beam physical vapor deposition
PIV	Particle image velocimetry
PDPA	Phase Doppler Particle Analyzers
OD	Optical density

Chapter 1

Introduction

In this chapter

This chapter will briefly introduce the thermal process and will focus on suspension plasma spray (SPS). Key parameters influencing the coating development and SPS applications will be presented. Moreover, a brief review of SPS studies, the significance of this work, and the objectives will be presented.

1.1 Introduction

Thermal spray is a technique that is broadly used in industry to improve the mechanical, thermal, chemical, or electrical properties of surfaces or add new desirable functionalities. Thermal spray is widely used to make thermal barrier coatings and to increase the resistance of surfaces against wear, erosion, and corrosion. Thermal spray can reduce the global cost of components and increase their life spans. Moreover, thermal spray was utilized to make microfiltration membranes [1] and hydrophobic surfaces [2]. More details about the thermal spray are described in the following section.

Thermal spray process

Thermal spray is as a group of coating processes in which fine metallic or nonmetallic materials in the form of molten or partially molten particles are sprayed on a substrate to form a coating. The fine particles melt by receiving the heat from an energy source such as a flame, electric arc, or plasma. Then the particles are accelerated in a gas flow from the torch toward the substrate. The thermal spray process can be applied with a wide range of materials that can be melted without any decomposition to deposit a coating. Thermal spray processes are grouped into different categories based on the source of energy provided for melting the coating particles [3].

Among different processes in thermal spray, plasma spray is widely used in the industry. A high-energy electrical arc is generated in the plasma torch between a tungsten cathode and a copper anode. The gas injected in the torch is heated and ionized by the electric arc, which leads to the formation of a plasma. A schematic of the atmospheric plasma spray process is illustrated in Figure 1.1.

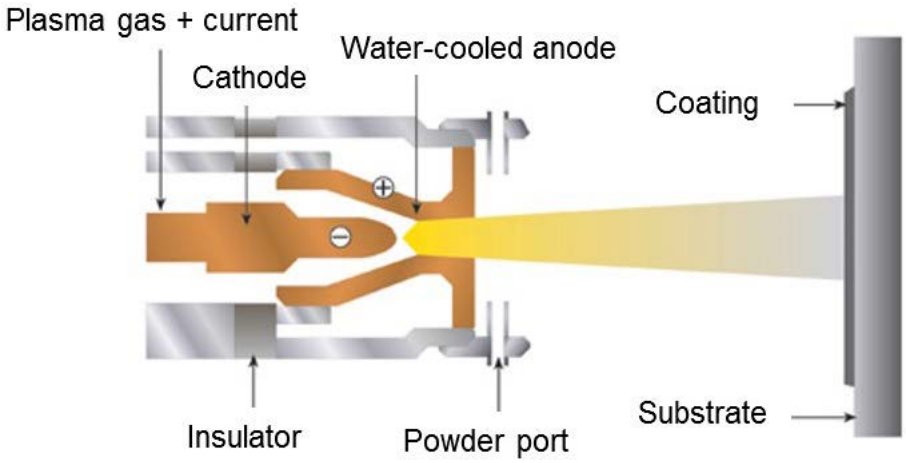

Figure 1.1: Schematic of an atmospheric plasma spray process [4].

The plasma gas can be Ar, Ar-H_2, or Ar-He-H_2. The temperature of the plasma jet at the nozzle exit can range from 8000 to 14000 K [5]. Figure 1.2 compares the particles' temperature and velocity ranges for different thermal spraying processes such as cold spray, plasma spray, flame spray, and high-velocity oxy-fuel (HVOF). The particles in the plasma spray reach the highest temperature compared to the other processes. However, the velocity of particles in plasma spray is relatively low.

In atmospheric plasma spray (APS), the size distribution of feedstock's particles is usually in the range of 10 to 110 μm [5]. A carrier gas is used to transport and inject these particles into the

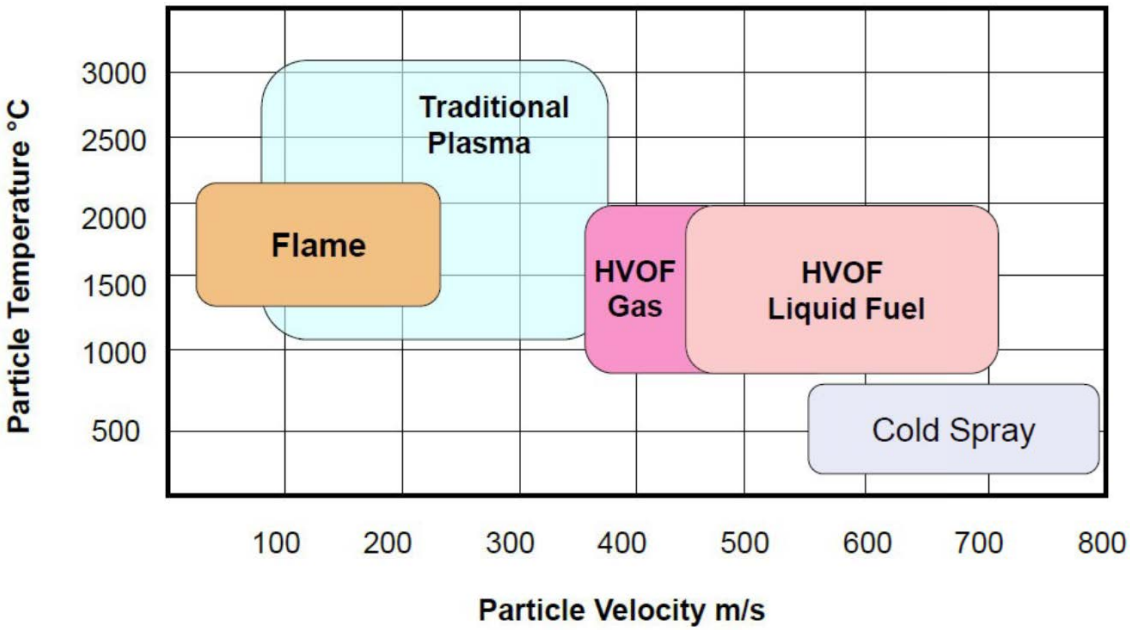

Figure 1.2: Particle velocity and temperature in different thermal spray processes [6].

plasma. Then, the particles are heated, accelerated, and deposited at the surface of the substrate.

1.2 Suspension Plasma Spray

Over the past decades, suspension plasma spray has been one of the most active research topics in the thermal spray. This process permits the deposition of coatings with better characteristics associated with the spraying of nano/submicron particles in suspension. The resulting finer microstructures create coatings with different noticeable properties such as lower thermal diffusivity, thermal shock resistance, wear resistance or improved catalytic behavior [7].

In the SPS technique, the feedstock suspension usually includes a solvent (water or organic liquids like ethanol), submicron particles, and a dispersant agent to stabilize the suspension [8]. The suspension could be injected radially or axially into the plasma plume as a liquid jet (mechanical injection) or a spray of droplets (atomization injection). After injecting, the plasma jet atomizes the suspension into fine droplets. Afterward, the carrier liquid evaporates by the heat flow from the plasma, leaving clusters of fine particles that would be heated and melted. The thickness of deposited coatings varies from a few microns to hundreds of microns [9]. Figure 1.3 displays a schematic of the SPS process [10]. It is helpful to highlight that droplets and particles define as a liquid phase composed of particles and molten or non-molten solid phases, respectively.

Various parameters might affect the coating microstructures like in-flight particles temperature and velocity, and size distribution. The injection properties of the suspensions in SPS play an essential role in coating development since it can affect the trajectories and thermal histories of the droplets into the plasma jet [11]. For example, Figure 1.4 shows that various plasma power effects to produce columnar structures with different inter-columnar voids and columnar features. In part b, the current intensity and plasma power were increased and result in forming a denser structure compared to part a. By increasing the current and plasma power, particle temperature and velocity

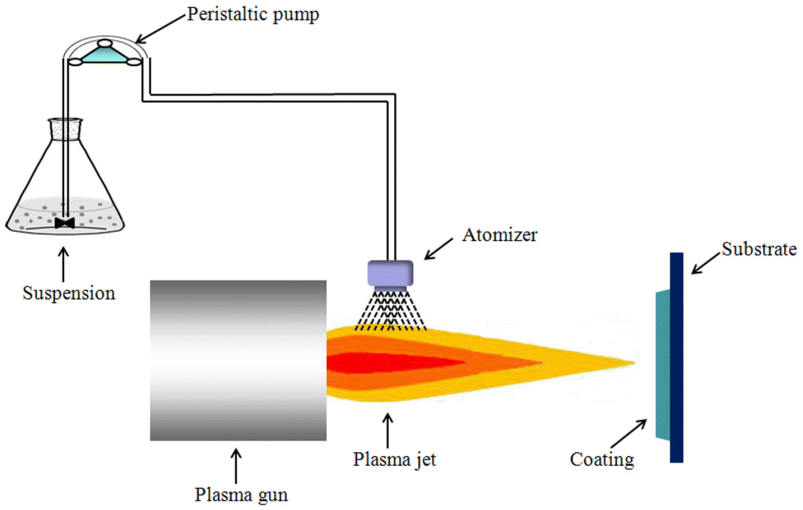

Figure 1.3: Schematic of SPS process [10].

increased, resulting in improving impact velocity and contact between flattened particles [12, 13]. Moreover, the enthalpy of plasma plume elevated, which can be led to particles melting during deposition. Thus, the enhanced bonding among layers and improved microstructure at high-power plasma can be achieved compared to low power plasma [14].

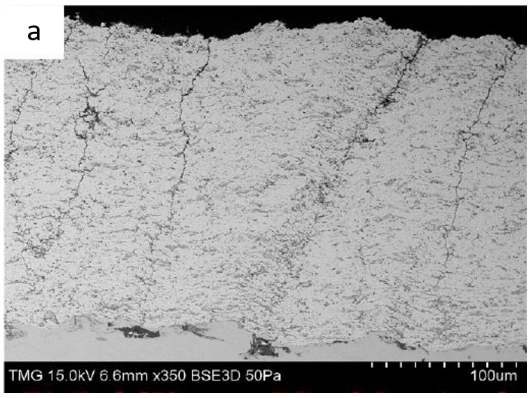

(a) SEM pictures of SPS YSZ coating microstructure produced with low power

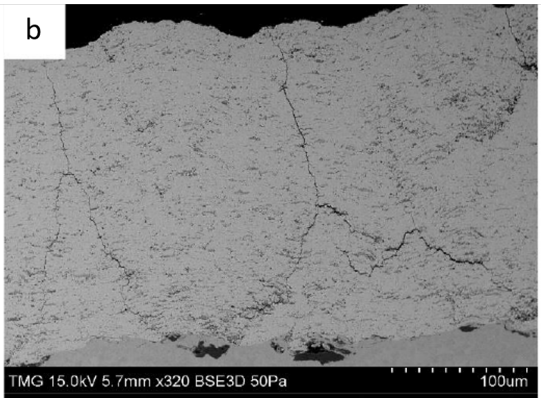

(b) SEM pictures of SPS YSZ coating microstructure produced with high power

Figure 1.4: SEM image of YSZ coatings cross-section deposited by SPS [14].

The columnar microstructure observed in SPS coatings can be described by the shadow effect. The small in-flight particles are entrained by the plasma flow, and their trajectories are deflected by the presence of the substrate surface. As illustrated in Figure 1.5, the trajectories of smaller and lighter particles are more deviated by plasma jet close to the substrate compared to large and heavier particles. Then the small particles are deposited at a shallow angle on the surface asperities. While the small particles tend to follow the gas flow, the larger ones pass through the boundary layer near the surface and deposit on the substrate [9]. The particles deposited at the surface and the columnar microstructure has grown from the surface's asperities due to a shadow effect [15]. The effect of shallow impact angles of particles results in the formation of columns and inter-columnar voids [14].

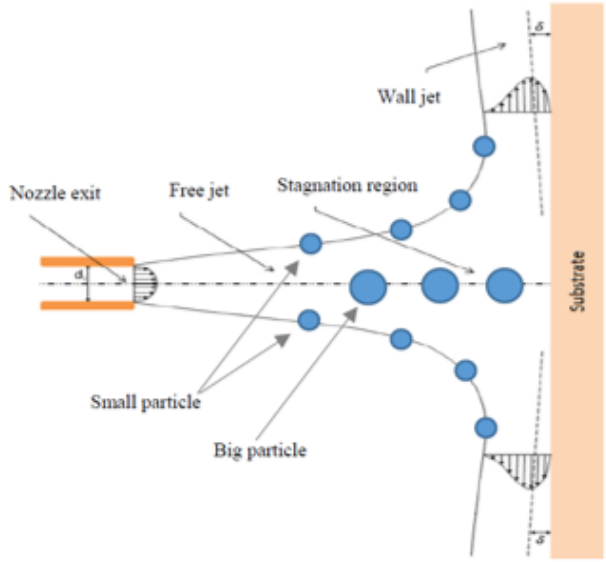

Figure 1.5: Schematic of a typical impinging gas-jet system [9].

As a matter of fact, the behavior of particles near the substrate can be characterized by the Stokes number for the in-flight particles.

$$St = \frac{\rho_p d_p^2 \upsilon_p}{\mu_g l}. \tag{1}$$

The Stokes number is the ratio of the particle's momentum response time to the flow-field time scale where μ_g, υ_p, d_p, ρ_p and l are plasma gas viscosity, dynamic viscosity, diameter, density of the in-flight particles, and boundary layer, respectively. A smaller particle with a Stokes number less than 1 tends to follow the flow field, while a particle with a high Stokes number follows its own trajectory. Figure 1.6 shows the result of the numerical simulation of a plasma jet with particles impinging on the substrate. It depicts how the speed of the gas and particles of different sizes is reduced in the stagnation region in front of the substrate [16].

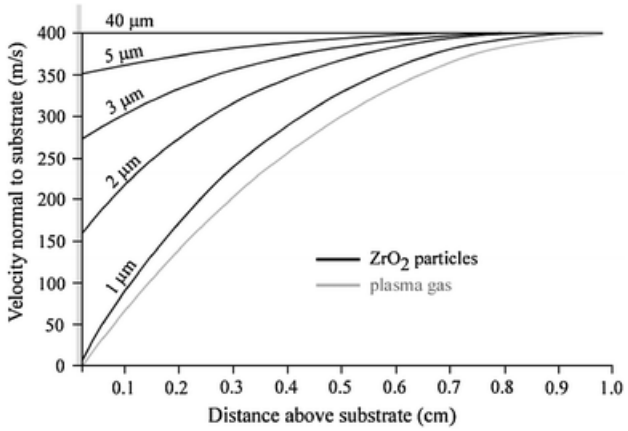

Figure 1.6: Replotted numerical result shows the effect of different diameters on normal velocity component [16].

As it can be observed, the speed of particles with diameters ranging from 1 to 5 µm is significantly reduced as compared to the speed of 40 μm particle (typical size in APS). Additionally, as they become smaller, like 1 μm, the particles have been more affected by the plasma gas and have roughly the same velocity as the plasma gas [15]. VanEvery et al. [15] have investigated the coating formation based on the trajectory of particles with different sizes near the substrate and shadow effect theory. Figure 1.7, illustrates the deposition characteristics occurring on and away from substrate surface asperities. In part (a) shows a high shadow effect made by smaller particles that have been influenced more by plasma jet and the particles accumulate on the external sides of the asperities. According to part (b), the momentum difference in larger particles leads them to deviate from the plasma trace-line at a specific turning angle. In Part (C), the shadow effect is disappeared since the trajectories of the impinging particles are not affected by the plasma jet. Therefore, they impact normally (90 degrees) on the substrate.

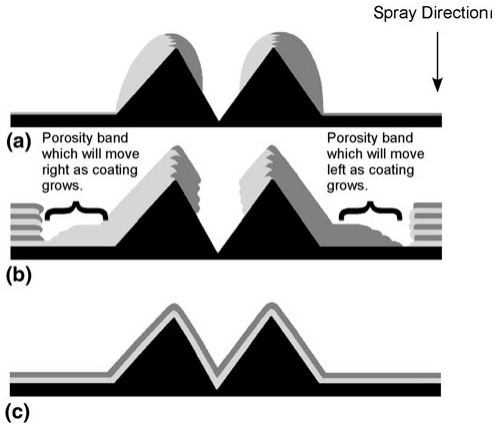

Figure 1.7: Schematics illustrating the deposition characteristics occurring on and away from substrate surface asperities [15].

In Figure 1.8, some different columnar microstructures in SPS coatings are illustrated [17]. These various SPS columnar microstructures can be applied in a wide variety of applications as discussed in the next section.

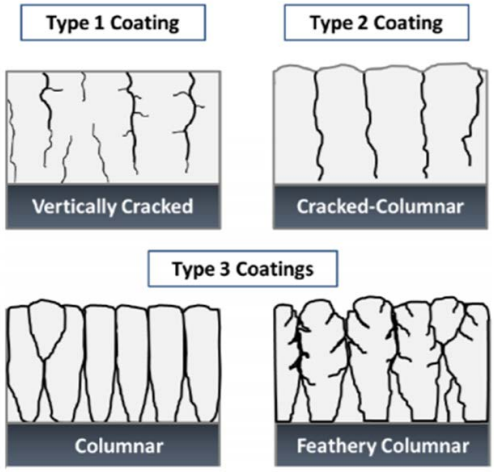

Figure 1.8: Schematic of different microstructures manufactured by SPS [17].

SPS coating applications

The columnar microstructures explained earlier can be used in solid-oxide fuel cells (SOFCs) for creating highly porous oxide structures [18]. These kinds of features are significantly crucial for a wide variety of applications not only in SOFCs but also in chemical sensors. SOFCs could convert chemical energy from fuels to electrical energy and heat by electrochemical reactions at the electrodes. The main issue of using SOFCs is its high operating temperature. As a solution, a columnar-like structure can apply to anode electrode as a coating to achieve low-temperature SOFCs with high stability [19]. Thermal barrier coating (TBCs) is one of the main applications of SPS coatings used in aviation and power generation to increase gas turbine engines' efficiency and the lifetime of hot components. They make it possible to increase gas turbines' operation temperature, resulting in significant performance improvements [20, 21].

TBC technology has progressed in two ways: (a) using materials with improved characteristics such as stability at a higher temperature, lower thermal conductivity, better thermal shock resistance and erosion resistance, and (b) using new deposition techniques [22]. Moreover, Microstructures play an important role in the case of thermal insulation and thermomechanical properties of TBCs. Applying low conductive materials with a high porosity level can result in low thermal conductivity. However, it should be ensured that the coating microstructure can relieve thermal expansion stresses and tolerate harsh conditions like thermal shock, high-velocity particles impacting, and high-temperature gradient [23]. Yttria Stabilized Zirconia (YSZ) is a promising ceramic material that has been widely used for TBC [24]. TBC coatings have been produced by various techniques, like Electron beam physical vapor deposition (EB PVD), APS, and SPS.

The role of different producing processes of APS, SPS, and EB-PVD in the performance of TBCs coatings is presented in Figure 1.9. As can be seen, SPS coating presents better TBCs performance and lower thermal conductivity due to the higher porosity of SPS coating compared to the EB-PVD coating. The high porosity microstructure and cone shape of SPS columns overcome heat conduction paths between columns and decrease the overall thermal conductivity. However, the lower porosity in APS causes higher thermal conductivity. The APS morphology cannot release thermal stresses as efficiently as SPS coatings resulting in a shorter life span [24].

SPS is one of the most promising methods to enhance TBCs characteristics among those explained earlier. However, mechanisms of growth of the SPS columnar microstructure are not yet completely understood. Moreover, particle size, temperature, and velocity can influence the development of the coating microstructure. In the next section, a review of some previous studies is presented regarding the significant parameters playing a role in controlling SPS coating structure.

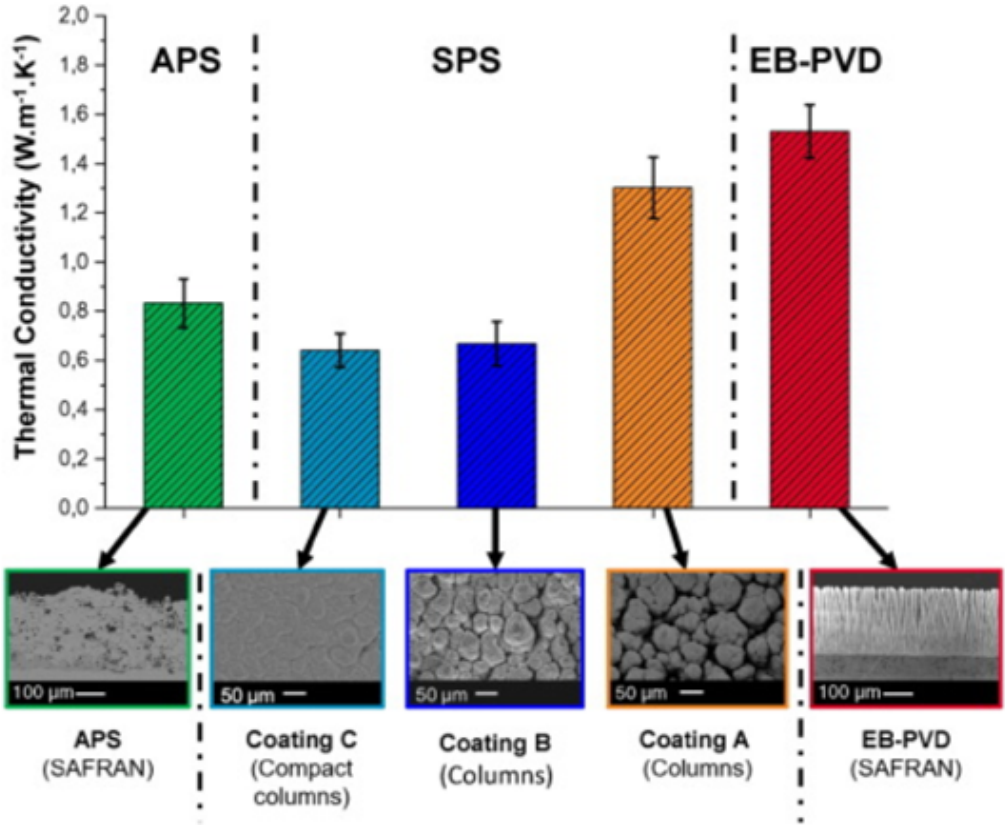

Figure 1.9: Thermal conductivities at 25 $^{\circ}C$ of YSZ samples coated by APS, SPS and EB-PVD [24].

1.3 Characterization Methods in SPS

Monitoring and controlling the effective parameters during plasma spraying are crucial in SPS to deposit superior microstructures. However, controlling of this process is more complicated than APS since there are several parameters that play an important role in the coating characteristics. Small particles with high speed and high temperature move toward the substrate to make the coating. The trajectory, velocity, size, and temperature of particles upon impingement on the substrate are key parameters that affect the growing coating structures. Therefore, understating and controlling these important parameters could be useful to develop repeatable, controllable, and desired coatings [25].

Recently, some numerical studies have been devoted to investigating and understanding this complex process by simulation of the plasma-particle interaction. Jabbari et al. [26] used three dimensional two-way coupled Eulerian-Lagrangian schemes to model the plasma flow and simulate the interaction between the droplets and plasma gas. suspension temperature, velocity, and trajectory were examined. Moreover, they analyzed the effect of distance on particles velocity, as the distance from the exit of torch increased, the number of particles with low velocity increased and result in increasing the porosity in the coating. The trajectory of particles near the substrate has also a significant influence on the deposition. Thus, some research has been devoted to studying the behavior of in-flight particles and fluid flow in the presence and absence of substrate. Kang et al. [27] investigated numerically and experimentally the effect of a flat substrate on the trajectory

of in-flight particles in APS. Their results indicated that adding the flat substrate has a significant influence on the flow field near the substrate and the zone affected by the substrate is relatively small about 5 mm. However, the trajectory of particles in the range of 22 to 125 μm remains mostly independent of the substrate position. To validate their result, the Spray-Watch (Oseir, Finland) particle diagnostics equipment has been employed. The captured pictures verified that the in-flight particles move towards the substrate without any significant changes in direction. Conversely in SPS, Jadidi et al. [9] have numerically simulated the behavior of the particles near the substrate at different standoff distances varying from 40 to 60 mm by using the same conditions and assumption used in [26] and concluded that fine particles could strongly be affected by the gas flow around the substrate. The particles could be deviated by the plasma flow in the stagnation region, especially at the shorter spray distances. In addition, Pourang et al. [28] analyzed the trajectory of zirconia particles near a flat and a curved substrate. As shown in Figure 1.10, numerical simulation results obtained from their work. [28] illustrated the effect of the insertion of a flat and a curved substrate on the trajectories of in-flight particles. In addition, the effect of stagnation flow on particle deviation was displayed. They concluded that the trajectories of smaller sized particles (below 2 μm) are more affected by the change of the flow pattern caused by the inclusion of substrate.

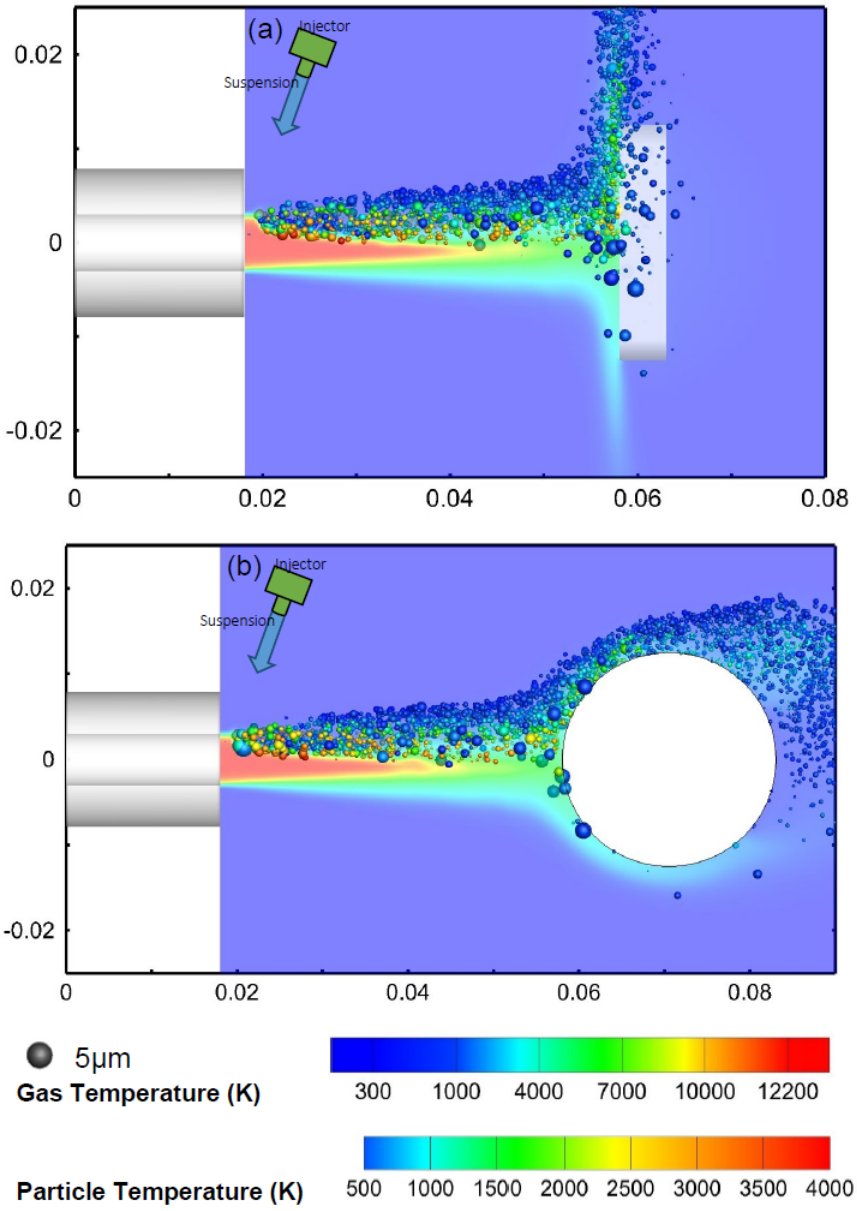

Figure 1.10: Plasma temperature contours with particle temperature including (a) flat and (b) curved substrate (dimensions in the above figure are in meters) [28].

As well as numerical studies, in experimental observation on growing coating, several models on coating development [17, 29, 23] confirmed the remarkable impact of particle behavior and velocity on the resulting coating morphology. In fact, impacting directions of these particles on a peak roughness create the columnar structure via the shadowing effect. Figure 1.11 and Figure 1.12 show different columnar microstructure obtained with various process parameters in SPS [17]. Columns with relatively large width growing in an off-normal direction or dense coatings (Figure 1.12 part b) can be obtained by varying the spray parameters.

Seshadri et al. [30] examined the effect of SPS process parameters like torch power and plasma

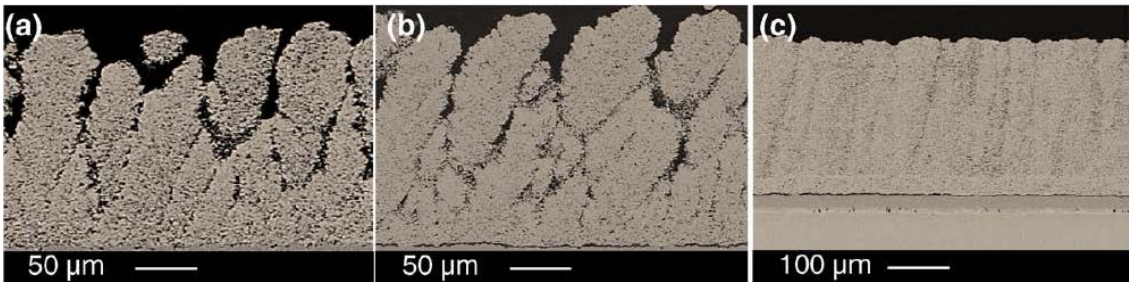

Figure 1.11: Different coating microstructures produced under different SPS process parameters with a low-power plasma torch with external radial injection [17].

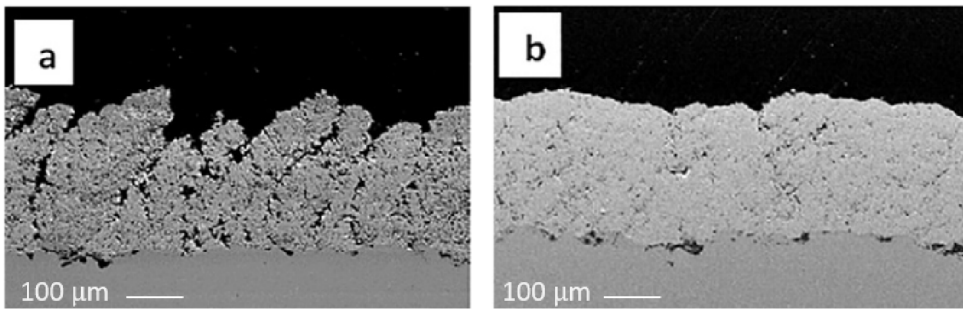

Figure 1.12: Different coating microstructures produced under different SPS process parameters with a high-power plasma torch with external radial injection [17].

flow rate on the microstructure of YSZ coating. Increasing the plasma power level, which could increase the plasma enthalpy, caused better melting of the suspension droplets to change the SPS microstructure from puffy columnar microstructure to a dense columnar microstructure, as can be seen in Figure 1.13. At low power conditions in the plasma spray, the atomizing effect is reduced, generating larger suspension droplets. It could reduce the energy for heating particles; therefore, unmelted large particles reach the substrate to produce porous coatings. 1.13.

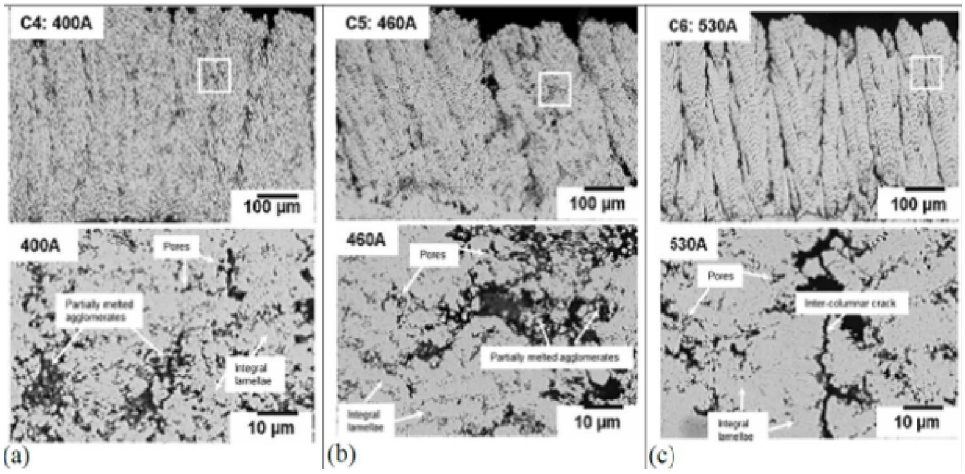

Figure 1.13: Effect of increasing torch power from low (a) to high (c) [30].

As observed in Figure 1.14, increasing the plasma gas flow rate lead to better atomization of the suspension, resulting in smaller molten particles. The trajectories of these smaller particles are more deviated closed to the substrate leading to larger gap between the columns due to the shadow effect [30]. Alongside the numerical and experimental researches mentioned above, online particle diagnostics in suspension plasma spraying has proven to be an interesting approach to develop a better understanding of the process to obtain a repeatable and controllable SPS coatings. In the next section, the importance of using such online diagnostic tools is briefly discussed.

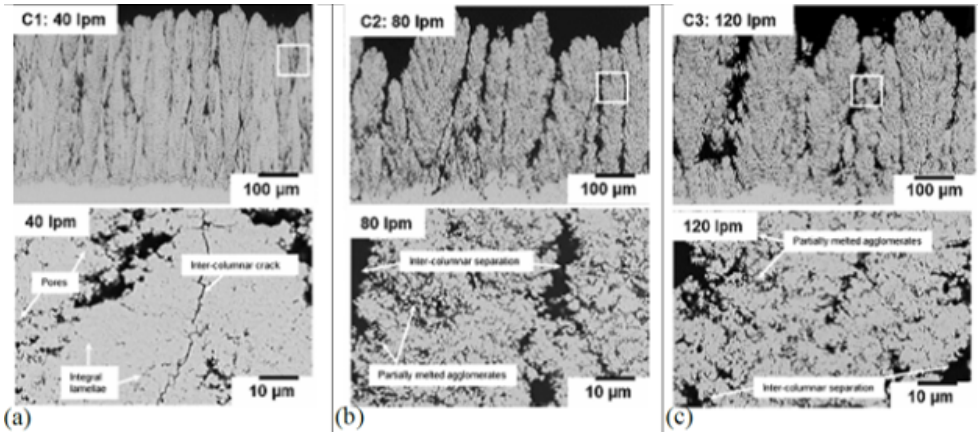

Figure 1.14: Effect of increasing plasma gas flow rate from low (left) to high (right) [30].

1.4 Particles and Droplets Diagnostics

In-flight particle diagnostics are recognized as practical techniques to monitor particle characteristics and injection parameters. Diagnostic tools help better understand the process to get control over the process and reach the desired coating reproducibility [31, 32]. Velocity measurement on in-flight particles is one approach. It can be carry out as a single-particle technique in which the velocity of individual particles is measured one at a time. Conversely, the measurement can be done simultaneously on an ensemble of particles [33]. The single-particle techniques require a limited measurement volume to avoid interferences from other nearby particles. While in ensemble measurements, the information is linked to many particles, and the techniques can be used with heavily loaded jets. Dealing with the particle characterization in the plasma jet (single particle or ensemble measurements), its impact on the substrate, the plasma jet monitoring, and its instabilities are critical parameters that need further investigation. The main goal of this work is to review the particle trajectory and velocity measurement of in-flight particles. Different diagnostic methods are used to measure the velocity of in-flight particles that the next section reviews some diagnostic approaches to carry out such measurements.

1.4.1 Particle Image Velocimetry

In particle image velocimetry (PIV), as the name expresses, the flow velocity is determined from the capture of consecutive high-speed images. Two consecutives images of the particles are captured in a plane illuminated by a thin laser sheet. From these images, the displacement of the particles during the inter-image time interval is measured and the velocity calculated. PIV can apply

to a range of liquid and gaseous flows. In most PIV applications, the flow is seeded with submicron particles, which are small enough to follow the flow dynamics and large enough to scatter sufficient light from the incident light sheet. The velocity of the particles is measured by the motion of particles. This calculation has been done by taking two images in a short time after one another. The displacement field is calculated from the seeding particle movement between the two images, and the velocity is gained by dividing the displacement between particles by considering the given time. A PIV system contains a laser, two high-resolution CCD cameras and a synchronizer [34]. More precisely, a CCD camera is placed orthogonally to the light sheet and the flow direction. Its shutter is synchronized to acquire an image from only one pulse of the laser. Then, two successive images are captured with a time delay over the period of the interest. The time delay should be selected based on the flow velocity and the magnification at imaging and it is generally on the order of a few μs except for slow-moving flow. For calculating the velocity field, those two successive frames are divided into a small sub-domain called the "integration window". Then the most probable displacement between the same particles in each interrogation windows can be calculated by cross-correlating of images of the particles in each interrogation area. Finally, the flow velocity field can be obtained from the measurement of displacement of imaged particles versus the determined time. Figure 1.15 shows the steps to record particle image velocimetry.

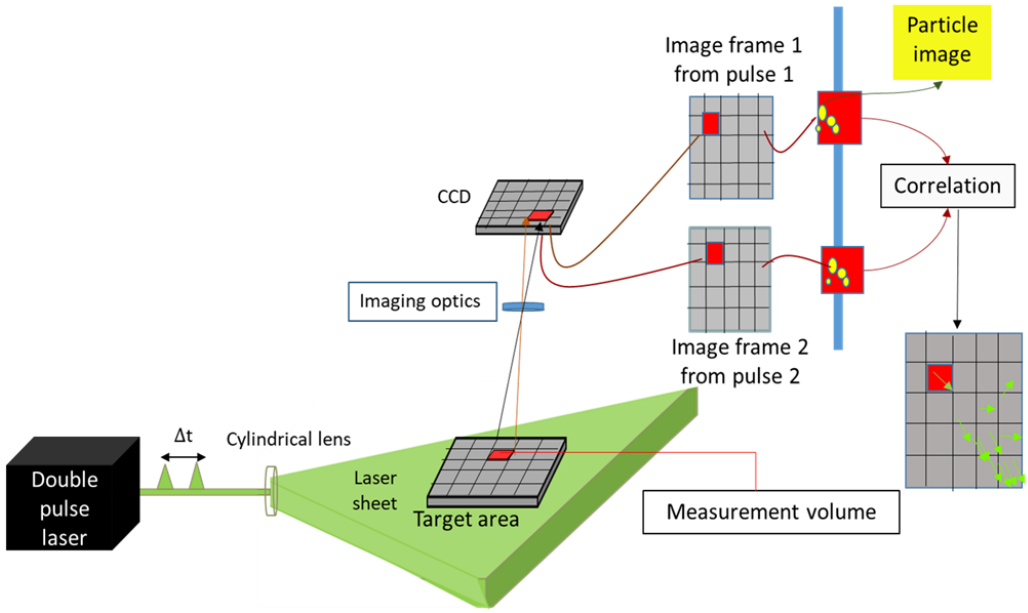

Figure 1.15: Schematic of particle image velocimetry set-up and steps. The laser created a laser sheet which illuminates the particles in the flow. Then the recorded images are subdivided into interrogation windows. Finally, in a given time, the velocity field can be calculated by cross-correlating the corresponded windows form one frame to another frame.

Figure 1.16 depicts the velocity vector field obtained from the PIV image of the whole spray jet with an ethanol suspension. It can be seen that the velocity increased along the torch axis from 150 m/s at 10 mm of the nozzle exit up to 450 m/s [34].

Particle image velocimetry is a non-intrusive method to obtain the velocity accurately. However, some parameters must be considered in order to get valid data such as magnification, seeding particle density, and time between the laser pulses. These are factors reviewed in detail by Keane et al. [35]. A brief description of these parameters are described below.

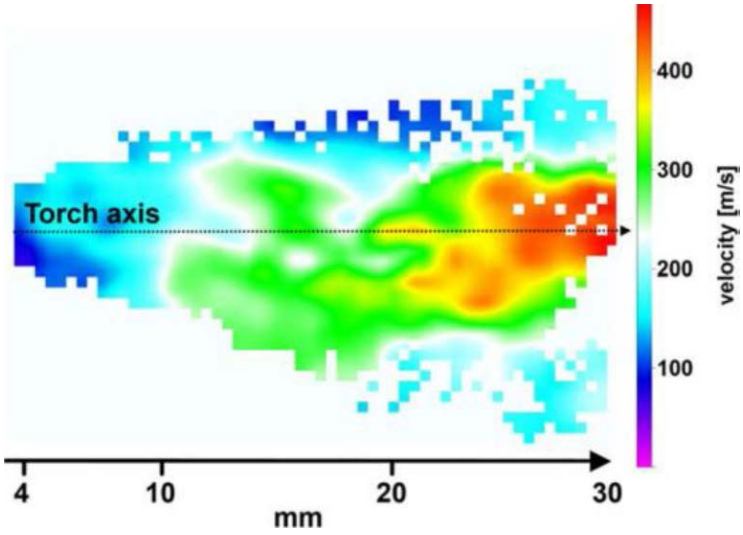

Figure 1.16: PIV calculated velocity vector field for the following plasma conditions: Ar 30 slim-H2 10 slim, I = 600 A, anode-nozzle i.d. of 6 mm [34].

Number of pixels that represents a particle, number density of particles in each interrogation, and interrogation size are important factors for a precise measurement. The particle diameters should be at least 3 pixels since the measurement of particle displacement is done based on the center of each particle image. An additional factor to consider is the seeding density, the number of particles used to seed the flow. For each interrogation region, the image density suggested to be between 7 to 15 particles. Furthermore, setting the time between the laser pulses is one of the most critical parameters that need to be adjusted. In general, the time is set based on the displacement of the particles, which should be roughly a one-quarter of the interrogation region size. For example, if the interrogation window size is 128×128, then the fastest particles in the flow move 32 pixels or less from the first frame to the second.

1.4.2 Thermal Emission Sensors

In thermal spray processes, particles are typically heated at high temperature. In this case, it is possible to use the thermal radiation emitted by the hot particles to measure their speed and temperature. The Accuraspray and DPV 2000 are two thermal emission sensors (TES) based on such an approach [32]. In the Accuraspray (Tecnar Automation, Canada), particle velocities are calculated from cross-correlation of signals that are detected at two closely spaced locations [36]. The system is consisted of CCD camera, a computer, analog signal processing unit and an optical detection assembly made of a collecting lens, two optical fibers, filters, and photodetectors as provided in Figure 1.17.

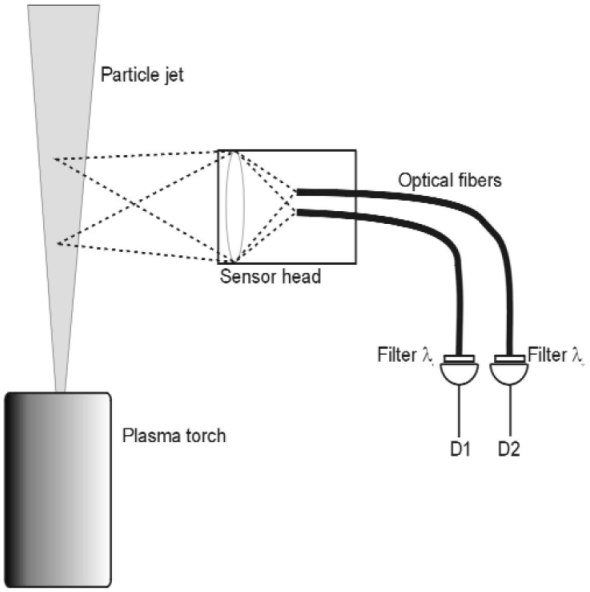

Figure 1.17: Optical arrangement for characterization of the particles in the Accuraspray [32]

In general terms, in the DPV 2000, in-flight particle velocity is measured by applying the time of flight methods. Each particle radiates a signal that passes through two slits, which are placed parallel to each other at a known distance. By knowing the time between two radiation peaks measured in each detector and the distance between two slits, the velocity can be calculated. Figure 1.18 illustrated the schematic view of the sensor head of the DPV-2000 used to monitor the in-flight particle properties like temperature, velocity, and diameter [32].

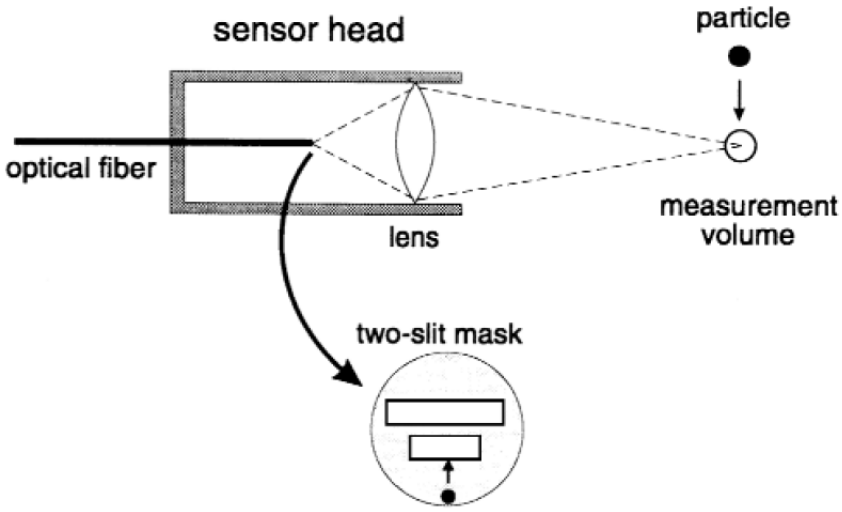

Figure 1.18: Schematic view of the DPV-2000 [32]

1.4.3 Phase Doppler Particle Analyzers

Phase Doppler Particle Analyzers (PDPA) is used to measure simultaneously the size, velocity, and concentration of spherical particles. It is typically used for liquid sprays, also some bubbles, and solid spheres. Since it can measure both the size and velocity of single particles at the same time it makes it possible to study correlations between these two quantities. This technique is also highly utilized to measure any liquid spray with transparent or semitransparent droplets. The system consists of a laser-based optical transmitter, an optical receiver, an electronic signal processor, and software to capture and analyze data. Droplets should go through the point that two laser beams meet each other. It creates a spray pattern; the pattern is produced by the interference between the two laser beams when a droplet goes through the intersection region of the PDPA laser beams. As the drop passes, the scattered interference patterns sweep past the receiver aperture at the doppler difference frequency, proportional to the drop velocity [37].

1.5 Challenges and Limitations of Diagnostics in SPS

Imaging and measuring optical signals for SPS has limitations and challenges. During SPS, Simple particle measurement techniques such as TES systems like DPV 2000 and SprayWatch are difficult to implement in SPS conditions. Indeed, the small size of the in-flight particles and their number density in the particle jet makes it almost impossible to detect individual particles. Since the small size of powder used in SPS and the limitation of diagnostics application in case of some features such as the size of particles and the spray distance, some specific measurement is necessary to evaluate in-flight particles' temperature and velocity in SPS [38].

In order to measure and observe the particle velocities and the particle trajectories, one diagnostic method is PIV. The advantage of using PIV compared to point measurement like PDPA is that it can capture the whole plane of the flow field at a specific time [37]. PIV has been already used in a few studies in the field of thermal spraying. It has been discussed in these studies that PIV is a useful diagnostic method to visualize and measure the particle velocity profile along the gun axis, which can lead to optimize the particles property parameter. The main outcomes of these studies summarized here.

Marchand et al. [39] examined the influence of the atomizing nozzle design and the gas-to-liquid mass ratio (GLR). Furthermore, the interaction of the suspension with the plasma jet has been investigated by PIV. TES has been implemented to validate the PIV measurement. By comparing between TES system and PIV under the same conditions [39], it was understood that the measurement between these two is different in the case of value. For different GLR, the velocity range obtained from PIV is between 113 m/s to 210 m/s, whereas in TES, the velocity has been changed from 410 m/s to 460 m/s [39]. PIV results correspond to the particle velocity, which is involved in the coating build-up in SPS process.

Aubignat et al. [40] suggested a methodology for characterizing a twin-fluid atomizer by using three diagnostic tools such as shadowgraphy, laser scattering, and PIV. The shadowgraph technique works based on high-resolution images with pulsed backlight illumination, which was employed to observe the liquid jet and suspension droplets in the plasma jet [34]. Laser diffraction and PIV were performed to measure, respectively, droplet size and droplet velocities. Figure 1.19 was recorded as an example of PIV images for injection visualization [40].

Finally, using these techniques, the influence of gas and flow rates on droplet size and velocity distribution was investigated. In addition, the optimum injection condition has been presented.

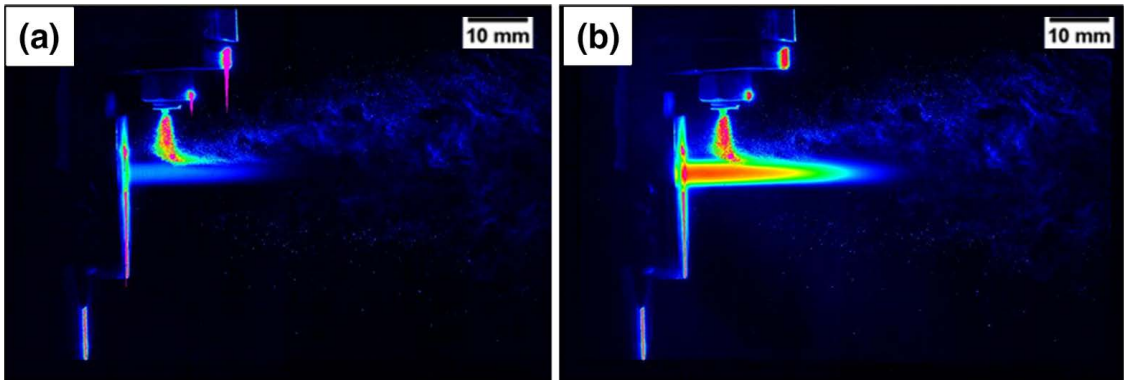

Figure 1.19: Example of a pair of images of injection visualization obtained successively with the PIV system: (a) the first image, (b) the second image, taken 200 ns after the first one [40].

Aubignat et al. [41] have investigated the effect of suspension properties on the development of coatings by SPS using an aqueous suspension and an alcoholic one. The suspension is injected by twin fluid nozzle that has been mentioned in their previous work. The in-flight particle velocity was calculated by PIV before the impact on the substrate.

Recently, Dolmaire et al. [42] studied the effects of the substrate shape and tilting on particle velocity, the direction in the vicinity of the substrate. PIV has been used to observe the behavior of the particles. They concluded different shapes of substrate influences on particle kinetic behavior and velocity of submicron zirconia particles. Their results reported that the particles impacting the cylindrical substrate (curvature radius of 25 mm) have higher velocity compared to particles impacting the flat substrate [42].

Accordingly, the previous studies agree on the developing microstructure in SPS directly corresponded to injection parameters, temperature, size, and velocity of the sprayed particles. Furthermore, the presence of the substrate has a significant effect on particle direction and velocity when impacting the substrate. In-flight particles' diagnostics are promising methods that lead to a better understanding of the process and control over the deposition to achieve a desirable coating.

The present work's motivation comes from the interest to investigate the effect of substrate on particle trajectories in SPS process. Among different diagnostic tools, PIV has been used to evaluate the SPS process. It can overview and visualize the whole field in the vicinity of the substrate compared to single point measurement. In addition, the flow pattern in the vicinity of the substrate can be observed, which cannot be possible with the other diagnostic tools.

1.6 Objectives

The main objective of the current study is to investigate the use of PIV as a mean to characterize the velocity field of SPS particles in the presence or not of a substrate. Such a study would help better understand the different phenomena characteristics of the SPS process and eventually better control it. The more detailed objectives of this work are summarized as below:

- Understanding the phenomena of the SPS process by visualizing the behavior of particles;
- Investigating the capability of PIV method to study particles in the vicinity of the substrate;
- Studying the effect of substrate on velocity and trajectories of in-flight particles;

Chapter 2

Methodology

In this chapter

An overview of the diagnostic tools and methods used in this work are presented. Furthermore, the experiment set-up and conditions are explained. This chapter consists of two parts. In the first part, the measurement technique is introduced. Then, the challenges of the experiment and the methods used are explained.

In this dissertation, experiments were carried out in two steps: (1) Setting up the PIV system with droplets generated with an oil atomizer and (2) Actual measurements in SPS conditions. The particles and flow were characterized by the two-dimensional and time-resolved PIV. The PIV was used with these specifications. A Nd: YAG laser was employed to create two collimated collinear beams, each with a pulse duration of 6 ns at a wavelength of 532 nm at a repetition rate of 15 kHz, and an energy of 120 mJ. Laser beams were created a 2D light-sheet with a thickness of about 500 μm. All the experiments performed are described in the following sections.

2.1 Velocimetry at Room Temperature

In this section, the set-up is developed at room temperature to examine the use of PIV as a method to characterize the velocity field of sub-micron particles with and without the inclusion of the substrates. Room temperature was used to address the challenges in the experiment for sub-micron particle velocity measurement. Plasma luminosity and limited access to control the PIV set-up are challenges caused by high operating temperatures which is up to 3500 °C.

2.1.1 Atomizer

Air or gas is blown through four holes in a tube into the liquid in the reservoir. These four jets then draw fluid up through vertical holes in the ring to create air bubbles containing finely atomized droplets. As the bubbles rise to the liquid surface, the droplets are released into the gas stream. Figure 2.1 shows the droplet generator schematic that is used [43].

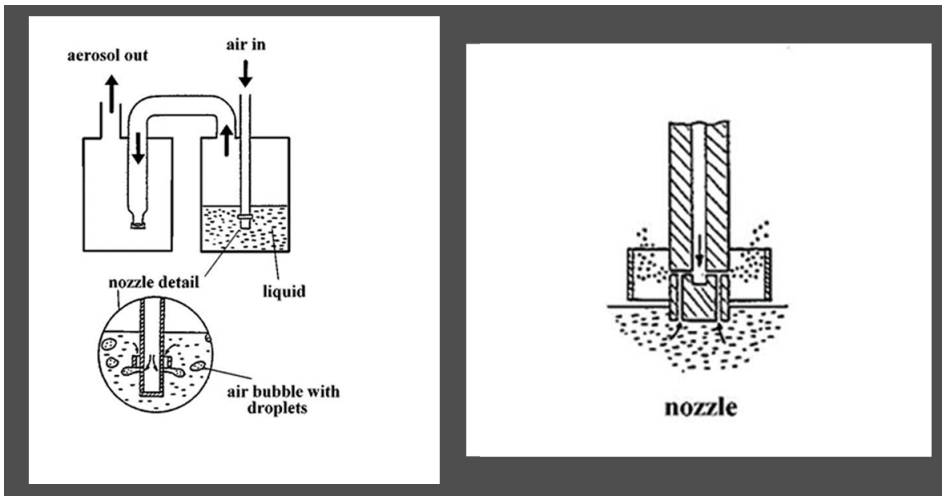

Figure 2.1: A Laskin nozzle citemelling1997tracer [43]

The oil atomizer is suitable to generate particles of sufficiently small size for PIV. These generators are typically used with olive oil but can also be used with other fluids such as e DHES (dioctyl sebacate, di(2-ethylhexyl) sebacate) or salt solutions (for aerosolizing solid salt particles). The oil is volatile, and it evaporates rapidly, and the vapors condense to fine droplets in the gas flow. In this section, some tests have been carried out at room temperature by using the oil atomizer with DHES as a seed particle. The advantages of utilizing the oil atomizer are creating a controlled distribution of small particles with diameter range from 0.5 μm to 1 μm. Moreover, it could make it more

controllable compare to a plasma gun (in case of noise, vibration, etc.). Furthermore, this material is quite more common for PIV to start the diagnostic then broaden to other materials like titanium dioxide (TiO_2) suspension.

2.1.2 Spray Characterization

A particle size analyzer, Spraytec (Malvern, UK), has been employed to measure the volume-based particle size distribution of particles produced by the oil atomizer. The spray is placed horizontally to the surface, as displays in Figure 2.2. The size of particles is measured at 16 points to ensure the particle's size distribution is uniform. These given points are defined in 2.1 by giving $(0, 0)$ as a reference. Therefore, the measurement has been employed at different points concerning the reference point.

Table 2.1: Given points in X, Y directions

(X,Y)	Y1	Y2	Y3	Y4
X1	(0,0)	(0,1)	(0,2)	(0,3)
X2	(1,0)	(1,1)	(1,2)	(1,3)
X3	(2,0)	(2,1)	(2,2)	(2,2)
X4	(3,0)	(3,1)	(3,2)	(3,3)

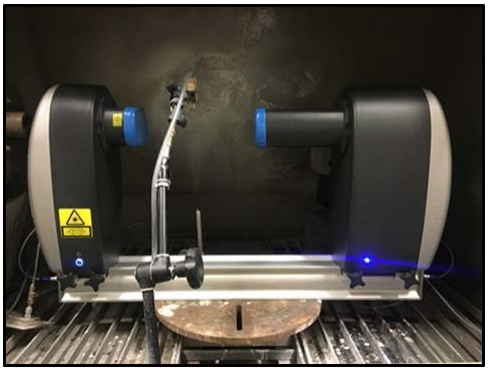

Figure 2.2: Spraytec set-up

The volume size distribution of three different points of measurement, point $(1, 0), (2, 1)$, and $(3, 3)$, displays in Figure 2.3. The results of volume-based particle size distribution at different points can provide the mean diameter of particle Dv $(50) = 600$ nm, which is fairly the same for these measurements. Thus, it can be demonstrated that the oil atomizer produces fine and uniform particles suitable for PIV and has the same approximate size of TiO_2 powder used in SPS.

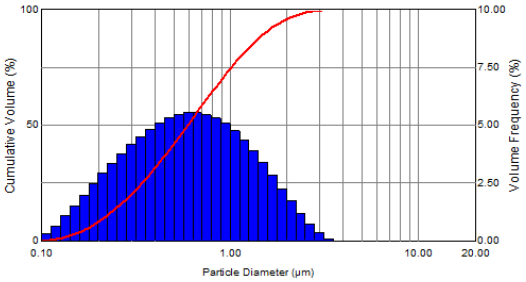

(a) the mean diameter Dv $(50) = 600$ nm at point $(1, 0)$

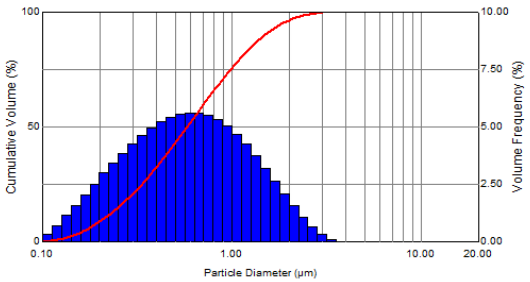

(b) The mean diameter Dv $(50) = 590$ nm at point $(2, 1)$

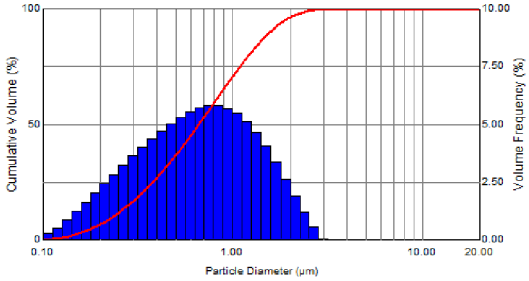

(c) The mean diameter Dv $(50) = 630$ nm at point $(3, 3)$

Figure 2.3: The volume size distribution for different points to observe the uniform size created by the oil atomizer

2.1.3 Room Temperature Test Set-up

In this dissertation, DEHS oil is used to fill a depth of about 2.54 cm in the atomizer device. When the liquid is added, it's ready to attach the pressurized air supply, a standard 100 Psi typically was used. The gauge pressure is then adjusted on 25 Psi to generate the small particles. In the first step, the velocity field characterization of the sub-micron particles without the substrate was performed at room temperature. Figure 2.4 displays the left side view of the actual set-up and the schematic for this experiment. The oil atomizer adjusted at the left side at 10 cm to the field of interest; thus, the flow with narrow size particles comes from left to the right; meanwhile, the laser is aligned with the oil atomizer and creates a laser sheet to illuminate the particles. The camera has been set on the top captured the red field with a size of 50×40 mm ^{2} to identify the velocity of sub-micron particles and visualize the particle directions in the free jet. It should be noted that the position of the oil atomizer, the camera and the laser sheet remained unchanged throughout all experiments reported in this dissertation.

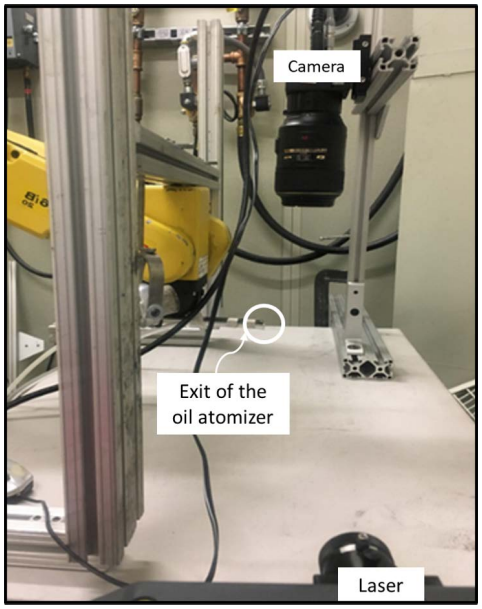

(a) Left view of the experimental set-up without using the substrate

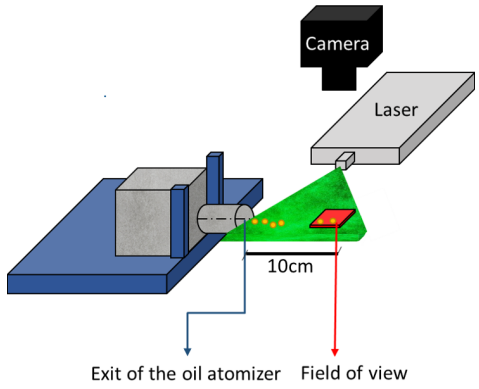

(b) The schematic experiment set-up without using the substrate

Figure 2.4: The left side view of experimental set-up without the substrate at room temperature by using the oil atomizer.

After examining the sub-micron particle velocities and directions, a few tests have been performed in the presence of the substrates to observe the effect of substrates on the deviation of sub-micron oil particles in the vicinity of the substrate. The left view of the actual set-up and schematic one is provided in Figure 2.5. The oil atomizer is located at 10 cm away from the substrate; then, the atomizer device is aligned with the centerline of the target and field of view. As identified, the sub-micron particles travel direction is from left to right. The laser created the laser sheet with a thickness of 500 μm to illuminate the particles. Additionally, the camera has been adjusted on the top and recorded the red field of view. The field of view is placed near the substrate to visualize the effect of the stagnation point on particle directions. However, at this point, different small windows were captured to provide enough magnification to observe the deflection of the sub-micron particles

near the substrate. The area of interest is addressed in detail in the following section.

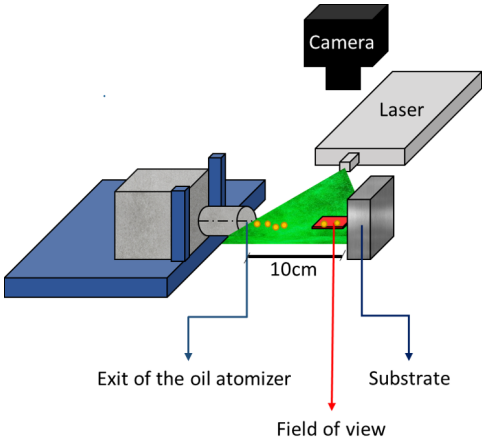

(a) The schematic experiment set-up in the presence of substrate

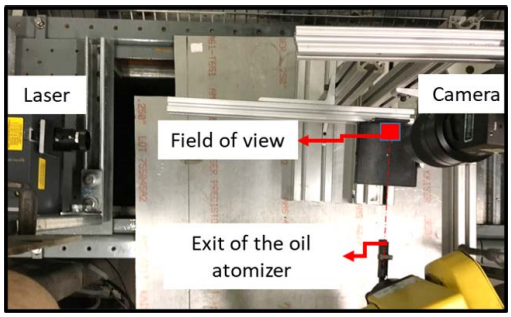

(b) Top view of experimental set-up in the presence of substrate

Figure 2.5: The experiment set-up in the presence of the substrate at room temperature by using the oil atomizer

2.1.4 Field of View

The CCD camera (model 630057 power view plus 2MP PIV camera) was used for capturing images with a macro lens (Nikon, Japan), the focal length is 105 mm, and the f-number is 2:8. The camera can record 32 frames per second at a maximum resolution of 1600×1200 with 12-bit image depth. Investigating the effect of the substrate on the flow and particle directions is one of this study's main objectives. The substrate has a significant impact on the flow and its turbulence behavior. Therefore, a larger area is required to characterize the particle directions and the stagnation point. In addition, since particles' size is small, it is needed to capture the small windows to have high resolution to catch the sub-micron particles. Consequently, combination of small windows should be considered to examine the broader field of view. Figure 2.6 (a), (b), illustrated the calibration image for each of the windows, with a size of 10 mm $\times$ 6 mm, and ten different areas of interest with the same size, overlapped with the neighboring windows. In part c, the overview of the area to the exit of the oil atomizer in the experiment is displayed.

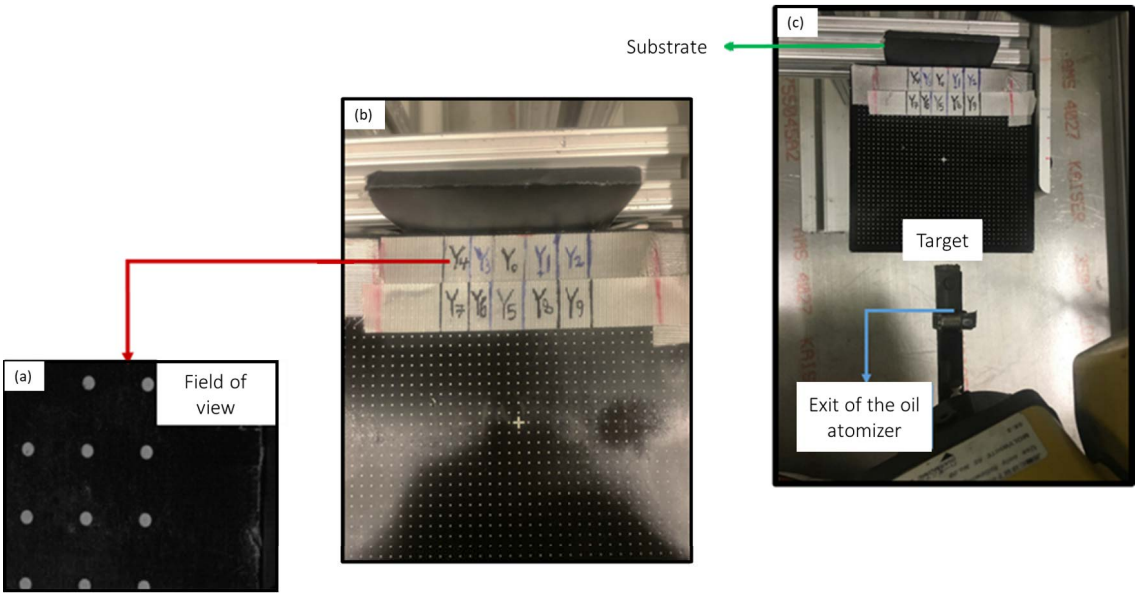

Figure 2.6: Different fields of view were recorded a) The calibration image for each of the windows. b) The view of 10 fields of views, c) Displays the robot's position to the area of interest.

2.1.5 Velocity Vector Calculation

For this study, a hundred pairs of images of sub-micron oil droplets were recorded with 10 μs between two consecutive laser sheets. One hundred images were captured to observe no additional flow variations in time and increase the velocity measurement accuracy. The background images were captured before the experiments have been carried out. Thus, the background images have been subtracted to enhance the light of images and equalize the intensity of light in the pairs of images by removing the background noise. In the next step, the velocity vectors were calculated by using a multi-pass approach with minimal smoothing. The advantage of using the multi pass approach was capturing the large particle displacements whereas using small interrogation windows. This method started with large interrogation windows to capture the full dynamic range of the displacements within the field of view by the one-quarter rule in low spatial resolution. Consequently, the displacement of the particles estimated and performed in the next higher spatial resolution, small interrogation windows. The multi-pass approach was performed starting from 64×64 px and ending with interrogation windows of 32×32 px. For these two passes, a 50% overlap between interrogation windows was applied, and the final grid dimensions are 0.581 mm $\times$ 0.581 mm and 0.343 mm $\times$ 0.343 mm , respectively, without the substrate and in the presence of the substrate.

In addition, the time interval between the two laser pulses should be small enough so that the particles stay in the laser sheet from frame one to the frame two to obtain an accurate evaluation of the in-plane velocity component. Keane et al. [44] and Adrian et al. [45] also identified a one-quarter rule for the out-of-plane velocity indicates that particles should move one-quarter of the thickness of the laser sheet within the laser pulses intervals. However, it is impossible to apply this rule without knowledge of the prior out-of-plane velocity component. Thereby, to evaluate whether the selected time duration is applicable in this regard, sample measurement can be performed to estimate the out of the plane component to find the proper time interval.

In PIV measurement, some spurious vectors may be observed during the evaluation process. A correlation peak was detected during the cross-correlating due to noise between two frames or artifacts such as model surface, out-of-plane motion, and the noise of different sources [46]. This incorrect data or spurious data points are often defined as outliers. Outlier vectors are defined as a data point different from the rest of the data based on the measurement, namely, a high correlation peak in PIV that is not obtained from the correlation of correct matched pairs. During computing velocity fields, outliers' vectors in the flow should be detected and removed. In general, in most applications, up to 5% or even to 10% of the vectors may be incorrect vectors, which is acceptable, according to [45]. In this case, less than 5% of acquired instances vector fields were spurious.

Throughout all the post-processing in Insight4G software, two approaches were performed to detect the outliers' vector. First, the signal-to-noise (SNR) vector validation was applied to eliminate the vectors with low signal-to-noise ratio during processing. SNR in the correlation plane is described as the proportion of correlation peak height concerning the mean correlation level. When the correlation did not pass, the SNR validation threshold was defined in the process; the vector was detected as an outlier and removed. The SNR criteria were set based on the monitoring of the process and the exported data in MATLAB. In this work, it was identified as 1.3. Furthermore, the median test is the second method to determine the outlier [47], which applied 2 times to the velocity fields to observe no additional outliers' vectors detected. The median filter is independent of the reference frame and magnitude of the flow velocities. It removes a vector based on whether its deviation from its neighbors' median is larger than the standard deviation. Then, eliminated vectors were replaced by using bilinear interpolation in MATLAB. The average velocity vector fields were computed and plotted in MATLAB.

2.2 Velocimetry in the SPS Process

In this step, the velocity characterization of the TiO_2 suspension with and without substrate inclusion was performed using the developed PIV set-up used at room temperature. In the present experiments, the suspensions injected into the plasma gas, and TiO_2 suspension were used as the seeding particles for particle diagnostic in PIV measurement. For this purpose, TiO_2 was chosen as suspension mainly based on highly used water-based suspension due to its chemical stability and abundance. Furthermore, it is cost-efficient and safe to do the studies. Particles were small enough to track the dynamic flow and large enough to scatter the light.

Direct radiation and reflection of plasma are the main challenges to do experiments by PIV for SPS process. At this point, a bandpass filter with a bandwidth of 10 nm and a different gray filter was used to remove the plasma radiation. The bandpass filter was used to pass the wavelength of 532 nm and block all the other wavelengths. In addition, gray filters with different optical densities (OD) have been employed to reduce the intensity in all wavelengths. Figure 2.7 a) and b) show the first pairs of plasma images with a bandpass filter 532 nm by the bandwidth of the 10 nm and gray filter with an OD of 0.3 to transmit of 50% of the light, respectively. In both cases, the plasma luminosity and reflection were still observed regarding using these specific filters. According to part c), the same bandpass filter and gray filter with OD $= 1.2$, which passed 10% of the light, were used. All the light and plasma radiation were filtered out using the gray filter with an OD of 1.5, which was not suitable for PIV measurement. In addition, the difference in light intensity between two consecutive images indicated that the second frame has a higher exposure time to be captured during the PIV. Figure 2.8 shows the timing graph for capturing two frames. For the first frame, the exposure time can be adjustable, while for the second one, the exposure time is fixed at 3000 μm to

save the image in this range, as shown in the figure. Therefore, the intensity of the two images is different.

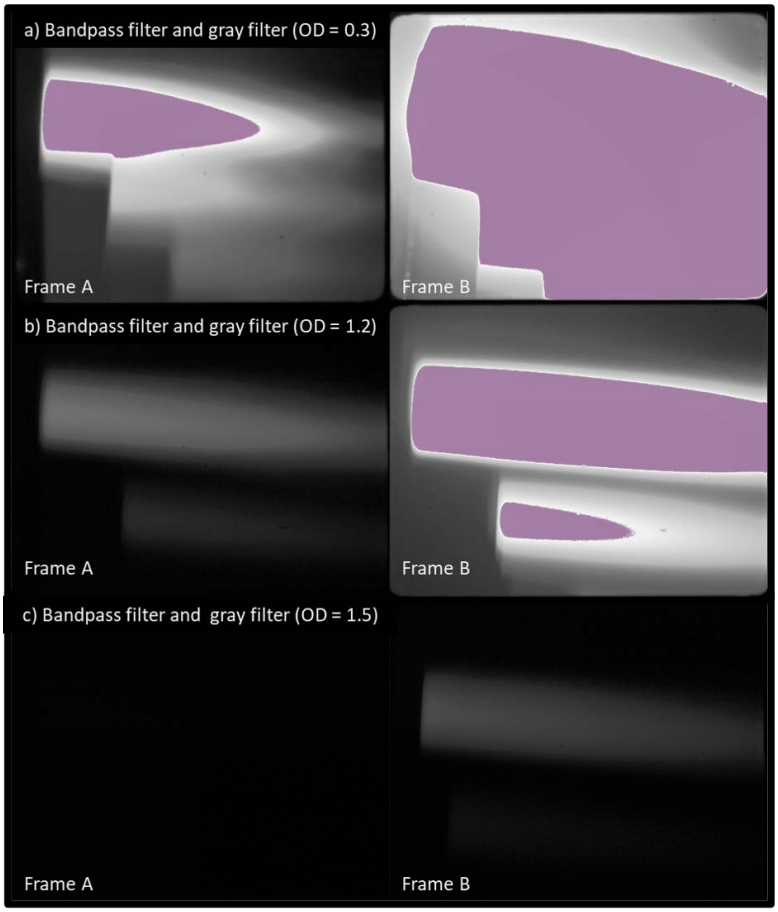

Figure 2.7: The first pairs of plasma images by using bandpass filter and gray filters

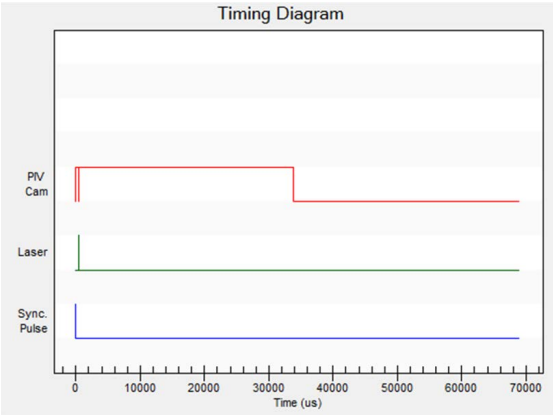

Figure 2.8: Timing diagram in PIV software

These observations indicate that different kinds of filters are needed to prevent the exposure of the camera from being dazzled by the plasma. In this case, a narrower bandpass with a bandwidth of 1 nm has been used to pass the wavelength of 532 nm and block all the other wavelengths, as displays in Figure 2.9 [48]. It should be highlighted that the range of transmissions of the selected filter was wide enough to accept tilted incident scattering up to 10 °. Additionally, the short pass filter is used to block all the wavelengths in the range of 610 to 1000 nm as shown in 2.9 part b. For wavelengths higher than 1000 nm, the CCD camera sensor, which was made of silicon, is negligibly sensitive to radiation in those wavelengths. And finally, a gray filter (OD = 1.2) has been used to reduce the intensity in all wavelengths. A raw sample pair of images using filters mentioned earlier illustrated in Figure 2.10. Part c) shows the application of a narrower bandpass with a bandwidth of 1 nm, low-pass filter, and medium gray filter as is an approach to filter out and enhance the images.

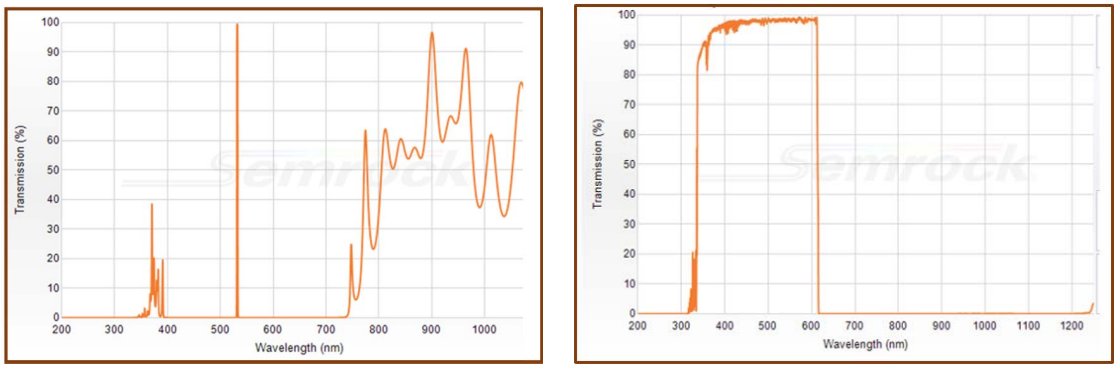

(a) Filter transition graph for bandpass filter

(b) Filter transition graph for the short pass filter

Figure 2.9: Filter transition graphs [48]

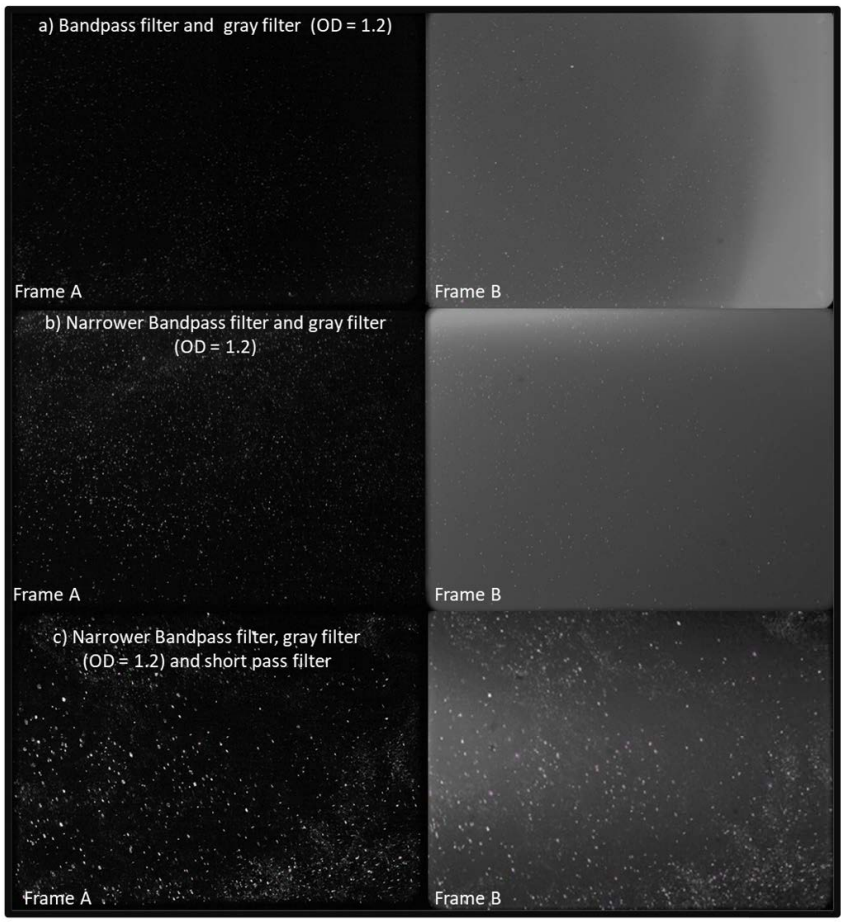

Figure 2.10: The first pairs of plasma images by using bandpass filter and short pass filters

Suspension preparation

TiO_2 (TKB Trading, US) was selected as the powder to prepare the water-based suspension. A suspension of TiO_2 particles was chosen to take advantage of its abundance and chemical stability and its use in different SPS applications. It can also be used as a seeding particle for PIV [43]. Water and ethanol can both used as a solvent for preparing the suspension. Other works presented more stability of water-based TiO_2 suspensions during the SPS process compared to ethanol-based suspension [1, 49]. In this regard, water-based was utilized as a solvent for preparing the suspension in this work.

To prepare the suspension of TiO_2 with a concentration of 10 %Wt. TiO_2 was dispersed in distilled water without adding a dispersant for 1 hr by using ultrasound at a frequency of 10 kHz to obtain a uniform and homogenization suspension. Additionally, to avoid agglomeration and uniform mixing, the suspension process has been done on the magnet stirrer by using sonicate to prevent large particles from agglomerating. The particle size distribution of the aqueous suspension obtained by a Spraytec unit (Malvern, UK) was Dv $(50) = 400$ nm. Figure 2.11 displays the result of volume size distribution and image of the as-purchased TiO_2.

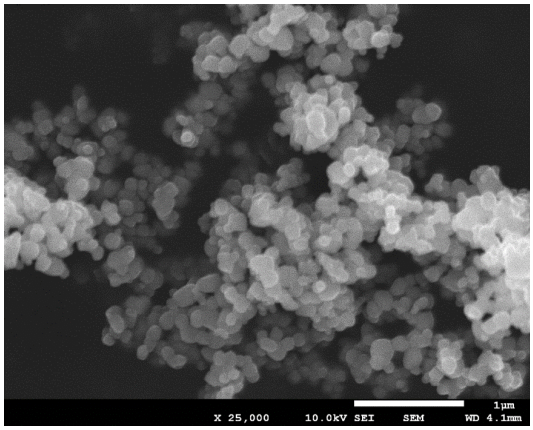

(a) SEM image the as-purchased TiO_2

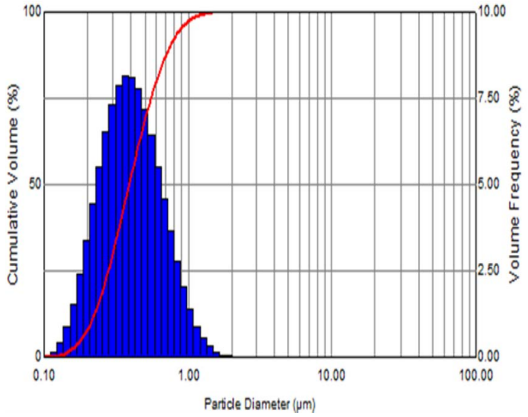

(b) Volume size distribution of TiO_2powder

Figure 2.11: The result of SEM image, and Volume size distribution

2.2.1 Experiment Condition

To spray the TiO_2, a 3 MB plasma torch (Oerlikon Metco, Switzerland) was utilized. The suspension was stirred in the pressurized tank with a magnetic inserted in the tank. Using a commercial suspension-feeding system (Northwest Mettech Corp., Canada), the suspension was injected radially into the plasma jet through an injector with diameter of 0.2 mm. The suspension flow rate was about 30 mL min^{-1}, and the flow rate and its density were monitored and kept consistent during the spray. Table 2.2 was addressed the spray conditions to describe more details about the spraying parameters.

Table 2.2: SPS coating parameters

Parameters	Set 1	Set 2	Set 3
Standoff distance (mm)	50, 60	50,60	50, 60
Feed rate (ml/min)	30	30	30
Hydrogen flow rates (NLPM)	0	2	2
Plasma power (kW)	13	25	25
Argon flow rate (NLPM)	50	50	50
Current (A)	350	500	500

Three different spray conditions at two standoff distances (D $= 50$ mm and D $= 60$ mm) were operated, given in 2.2. In both set 1 and set 2, distilled water has been used to modify the PIV set-up at the safe mode in case of spraying the distilled water to set the camera to prevent any damaging to set-up, and in set 3, TiO_2 suspension was used. In more detail, first, the experiments were operated with a plasma power of 18 kW at low power to adjust the set-up and calibrate the system. Then, selected filters mentioned earlier were adjusted to avoid the plasma radiation and reflection at the TiO_2 spray conditions with plasma powers of 25 kW. Finally, after aligning the set-up and filters via water, TiO_2 suspension was inserted in the pressurized tank while the magnetic stirrer mixer was put beneath to avoid sedimentation issues. Then, the suspension was injected at 8 mm from the nozzle to the plasma jet with plasma powers of 25 kW. Figure 2.12 shows the schematic of the radial injection that is utilized in this dissertation. It should be noted that during all the experiments,

the feedstock injection was radial.

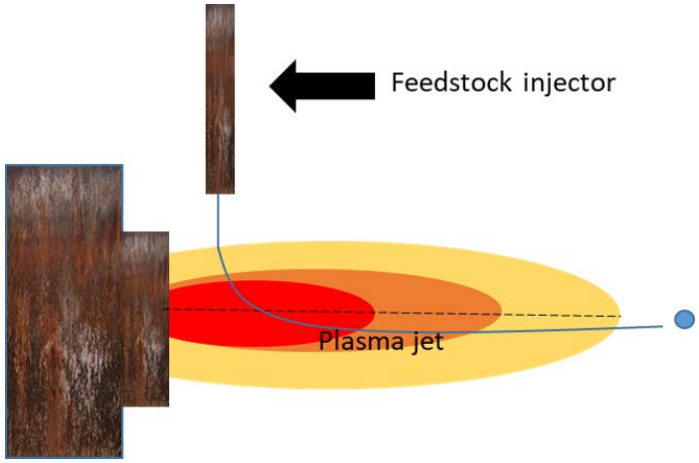

Figure 2.12: The Schematic of radial injection

In the first step, the particle velocities have been investigated in the free jet without any substrate. Figure 2.13. displays the front view of actual set-up and schematic for this experiment. The beam light dump is located in front of the camera to eliminate the radiation reflected out of the beam dump. Moreover, the actual set-up front view depicts a plate used as plasma protection to block all additional radiation entering the camera sensor to enhance the final image and the camera protected from suspension in the box. As it has been viewed on the schematic picture, the laser is located at the bottom stage and created the laser sheet with 500 μm thickness to illuminate the particles. The prism is placed ahead of the laser. It shifts the laser sheet to the front of the camera, set orthogonal to the flow. It should be noted that the position of the camera and the laser remained unchanged throughout all experiments reported in this dissertation.

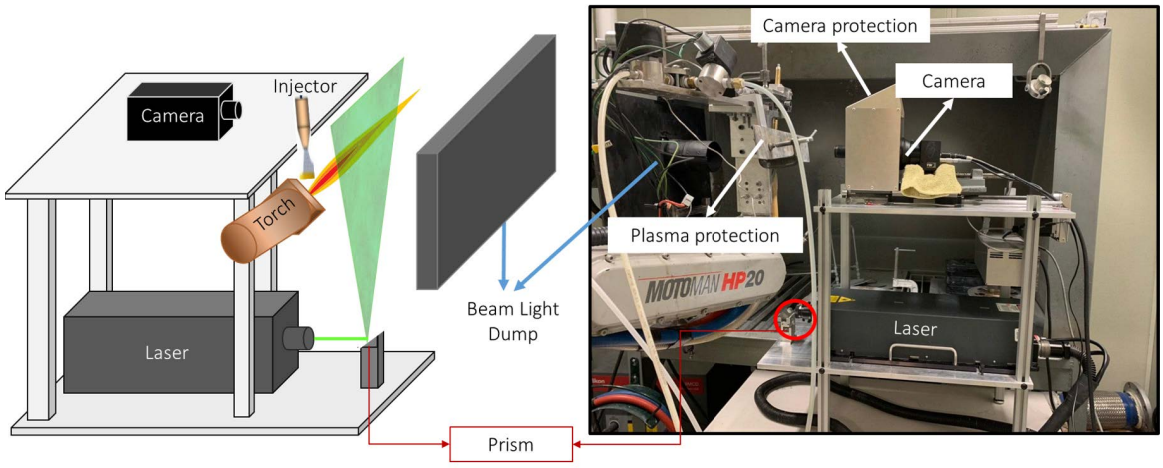

Figure 2.13: Left view of the schematic experiment set-up, and the actual set-up front view experimental set-up

Figure 2.14 (a) displays the configuration of the filters mounted on the camera in the SPS process, including the measurement section, laser sheet, bandpass filter, gray filter, and low pass filter. In part (b) shows the target located at the center of the torch and the start position (50 mm to the nozzle).

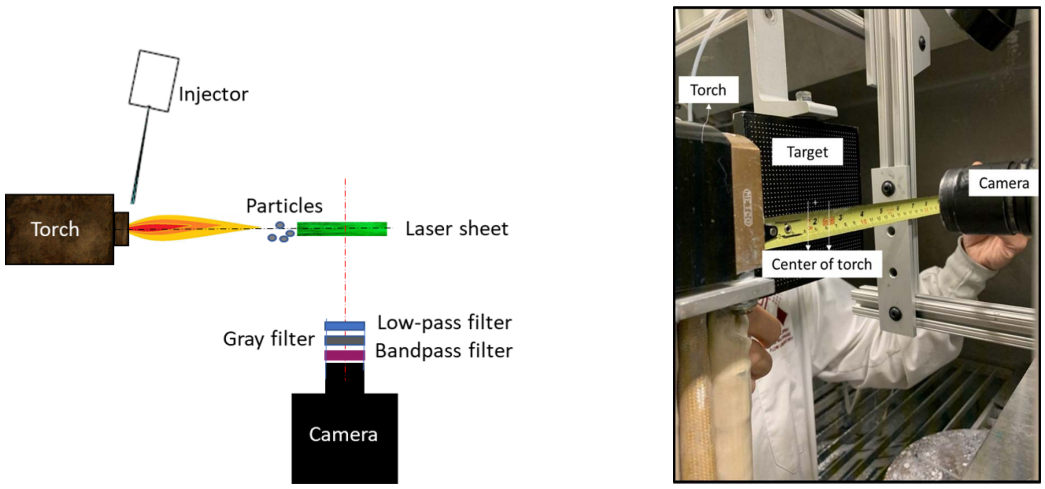

(a) Schematics of configuration of the filters in the set-up **(b)** Target at the start position (50 mm) to exit of the nozzle

Figure 2.14: The top view of the schematic of test set-up with configuration filters mounted on the camera and location of the target at the centerline of the torch at the actual front view

The velocity of particles has been investigated at the standoff 50 mm and 60 at different positions of windows, as shown in Figure 2.15. These different positions are selected at the center of the torch, then at 9 mm and 18 above and below the centerline. The measurement was carried out around the centerline of spray where there were enough particles far from turbulent regions.

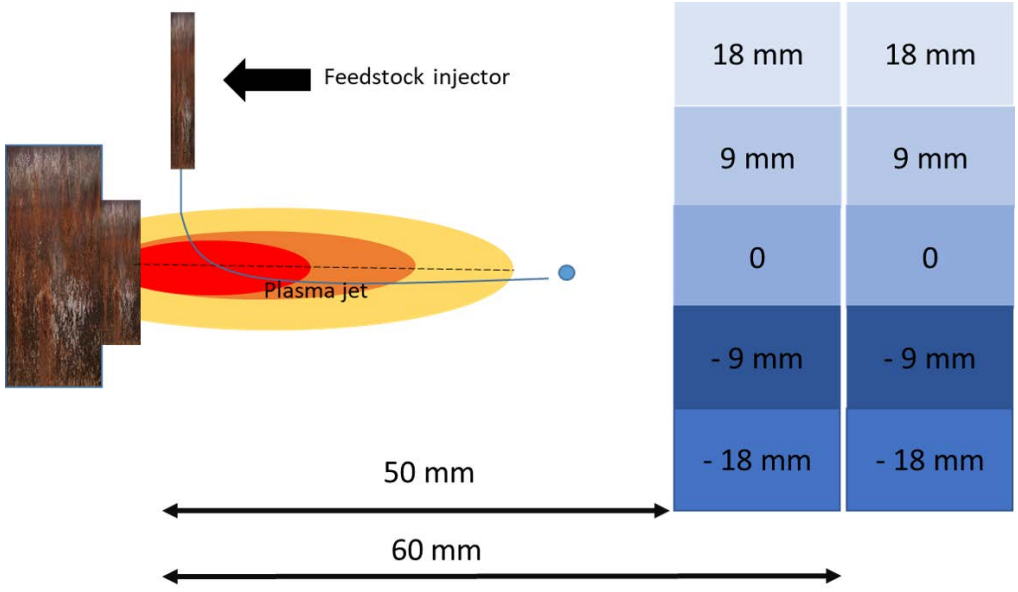

Figure 2.15: Schematic of the interested area at standoff 50 mm and 60 mm to exit of the nozzle

The velocity vector field of TiO_2 suspension has been examined in the free jet. At this point, some tests have been performed in the presence of the substrate to apprehending the influence of the substrate orientation on the flow behavior. Figure 2.16 shows the schematic of test set-up and the actual set-up in the left view. The location of the substrate was fixed around the interest area, and the torch was aligned at standoff distance 45 mm to the substrate. The camera has been adjusted to be perpendicular to the plasma and laser sheet. During the PIV measurement, the torch moves along the vertical axis to prevent melting the substrate.

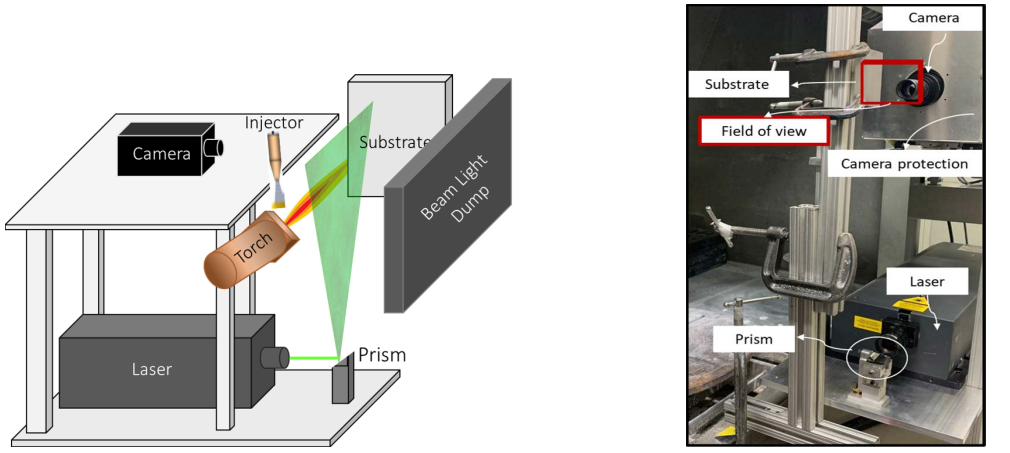

(a) The schematic set-up in the presence of the substrate

(b) the left view of the actual set-up

Figure 2.16: The experiment set-up in SPS in the presence of substrate

2.2.2 Field of View

The dimension of the field of view without and with the substrate, respectively, is about 12 mm $\times$ 8 mm and 25 mm $\times$ 20 mm. In the presence of substrate, a larger field of view is needed to observe the effect of the inclusion of the substrate on particle velocities and trajectories in SPS. Two fields of view are provided in Figure 2.17.

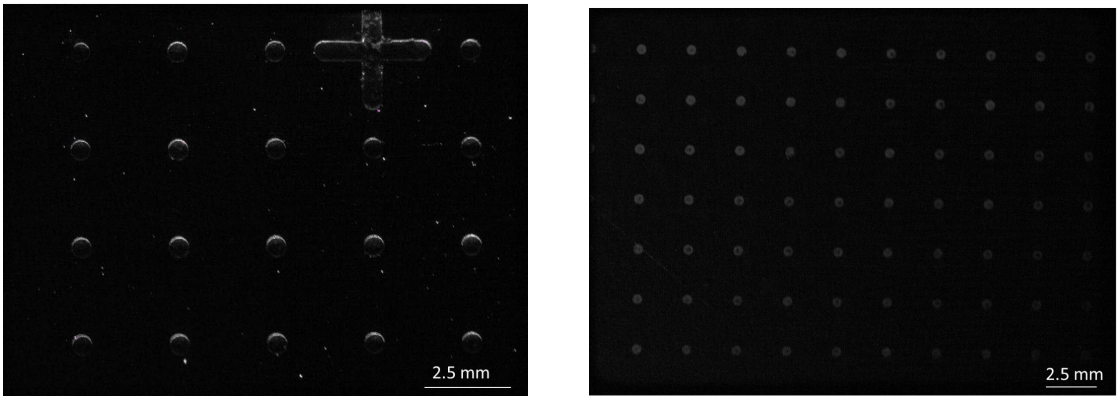

(a) A field of view in the free jet

(b) The field of view in the presence of substrate

Figure 2.17: Field of view in SPS

2.2.3 Velocity Vector Calculation

In this part of the study, a hundred pairs of images of TiO_2 suspension in plasma gas were captured with interval time 2 µs between two successive laser sheets. The velocity vector was calculated from these hundred images with an Eulerian method using PIV software Insight4G. In the Eulerian method, the velocity vector field V (x, y) of the flow pattern was calculated. In this PIV measurement, the laser sheet is fixed at a specific position (x, y) to investigate the flow pattern and particle behavior over the determined field. Thus, its output describes the Eulerian velocity field V (x, y, t). The same approach in the oil atomizer section was employed with different grid sizes to calculate the velocity. More precisely, two passes with a 50 % overlap between interrogation windows were performed to an initial pass of 128×128 px and the second pass of 64×64 px in the free jet and the presence of the substrate. The final grid dimension is 0.42 mm $\times$ 0.42 mm for both cases. To prevent duplication in the dissertation, the vector validation has been performed like the oil atomizer section. SNR vector validation and median test were used to identify the outlier vectors and remove them. Then, bilinear interpolation in MATLAB is used to replace the removed vectors. In this study, less than 5 % of acquired instances vector fields were spurious. All the velocity vector fields were computed in MATLAB.

2.2.4 Repeatability and sensitivity analysis

To verify the repeatability of the experiments, particle image velocimetry recordings were repeated for three times. The spray working conditions and position of the set-up components (camera, laser sheet, the torch, etc.) were all the same for the experiments. The deviations in the velocity vector fields were detected between 6 and 8% when comparing to the average velocity in 100 images. The general measurement errors in PIV, including particle image size, intensity, and density, velocity gradients, noise level, and interrogation window size, may impact on the uncertainty. The errors caused by set-up components, alignment, and the flow itself should be considered. In particular, the slight displacement in camera position and laser sheet should affect the sensitivity of the results. Moreover, velocity fluctuations in turbulent flows can lead to measurement errors that are acquired to be considered [46]. In this study, the experiments and measurement set-ups were optimized to ensure that the required flow information is captured as best as possible. Throughout the studies, the same recording plane was utilized, and the particles stay in the focus of the camera. Additionally, the camera distance was optimized to reduce uncertainty. Optical components like glass windows and filters may lead to reduce the sensitivity of the results. In this work, the holder for filters has been used to ensure that all the filters fix and aligned.

2.3 Velocimetry by PIV vs. Thermal Emission Method

As already mentioned in the previous chapter, several diagnostic techniques have been implemented to acquire the particles' velocity in the SPS process. In this study, TES was selected to measure the velocity of in-flight particles in SPS process, among the other tools. The reason is that it can be able to measure the ensemble particles. It has been applied in the same condition as the PIV performed. TES set-up is provided in Figure 2.18 . The green point is the measurement point, and it is placed at the same distances (D $= 50$ mm and D $= 60$ mm) to the exit of the torch that PIV has been run.

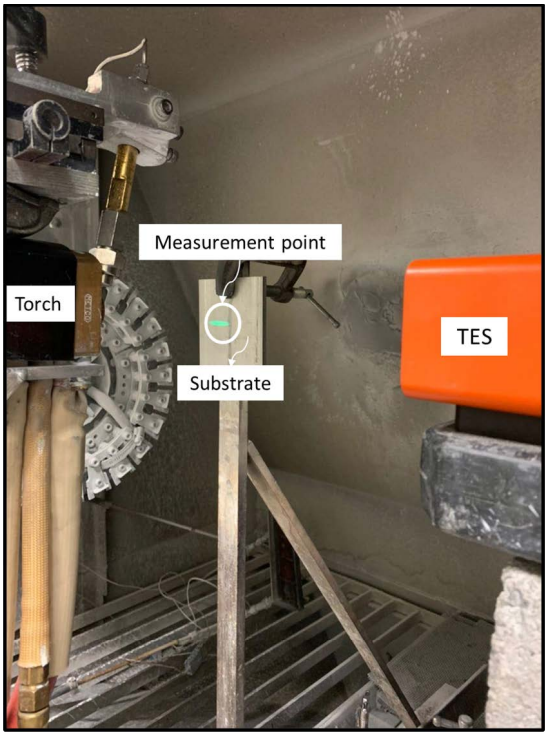

Figure 2.18: TES set-up in SPS

Chapter 3

Results and Discussions

In this chapter

PIV measurement results at room temperature and plasma conditions with and without inclusion of a substrate are presented. The velocity and trajectories of in-flight particles in suspension plasma spray are visualized in both free jet and with the substrate.

3.1 Room Temperature Case

3.1.1 Free Jet

Particles' velocity and trajectory has been studied at room temperature by atomizing DHES particles to develop the PIV set-up at room temperature and verify the measurement system used in SPS process. Particles' velocity and trajectories have been investigated with and without the substrate. Figure 3.1 presents the velocity vector field for the free jet at room temperature. The PIV measurements demonstrate the DEHS particle movement along with the gas flow. According to the size distribution mentioned in chapter 2, the DHES particles produced by the oil atomizer are fairly uniform and well-dispersed in the measurement window. Therefore, these sub-micron particles attain velocities up to 50 m/s, the same as flow velocity measured by a pitot tube. The uniform size of sub-micron particles resulted in the same average velocity in the selected window.

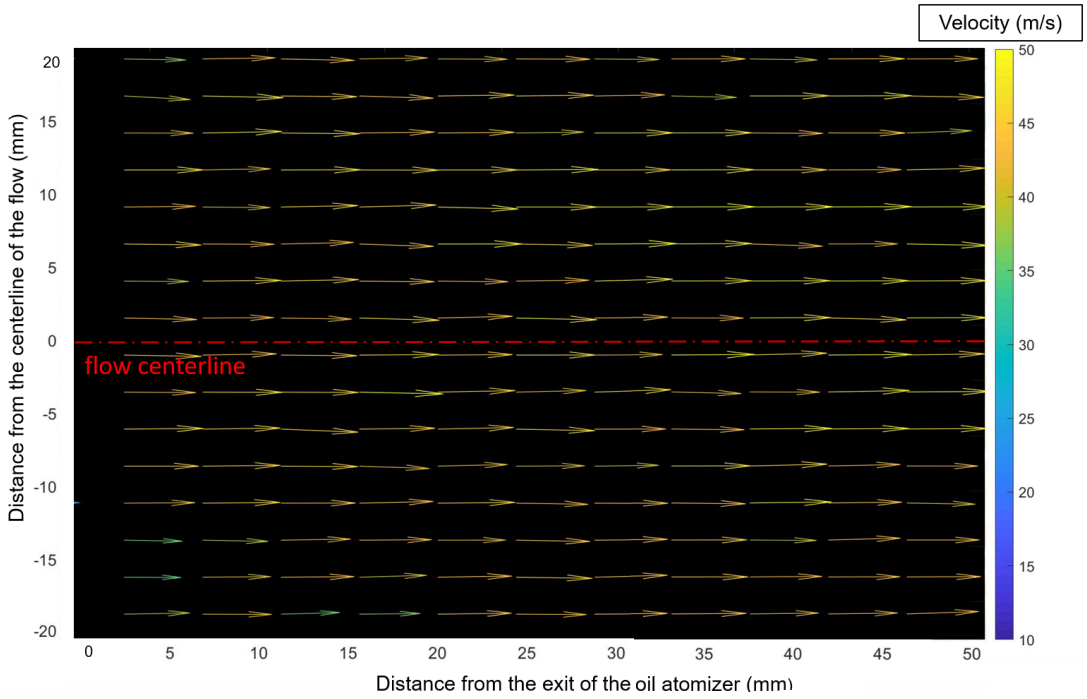

Figure 3.1: Velocity vector field for free jet at room temperature.

3.1.2 Stagnation Flow

The focus of this study is to investigate the effect of the substrate on the in-flight particles, specifically in the vicinity of the substrate like stagnation flow. PIV measurements have been employed in the collage of different windows in the vicinity of a substrate. In Figure 3.2, the area of interest is visualized and corresponded to the instantaneous velocity of the particles. The deviation of particles near the substrate shows the effect of the substrate in the particle direction.

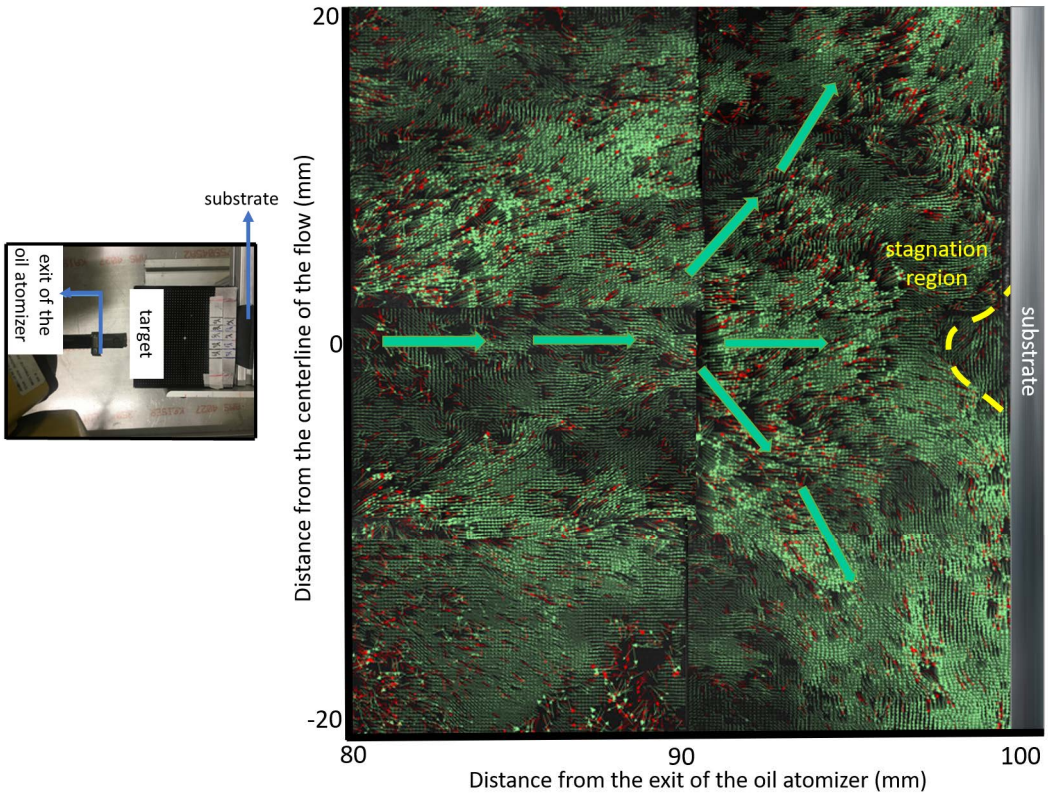

Figure 3.2: Superposition of velocity vector fields in the presence of the substrate, left picture shows the view of set-up and showing the direction of the flow

This observation indicates that the velocity of sub-micron particles is sensitive to flow direction, and particles strictly follow the gas flow streamlines.The deviation of flow was captured by PIV. Figure 3.3 presented that the sub-micron particles start to deviate at 10 mm away from the substrate. Moreover, the relative velocity could be acquired before deviation and after deviation. The average particle velocity measured in the middle of the free jet flow is about 50 m/s. However, the particle velocity decelerated in the vicinity of the substrate due to the stagnation flow, as shown by the yellow dash line in Figure 3.2. Particle deceleration in the presence of a substrate is provided in Figure 3.3.

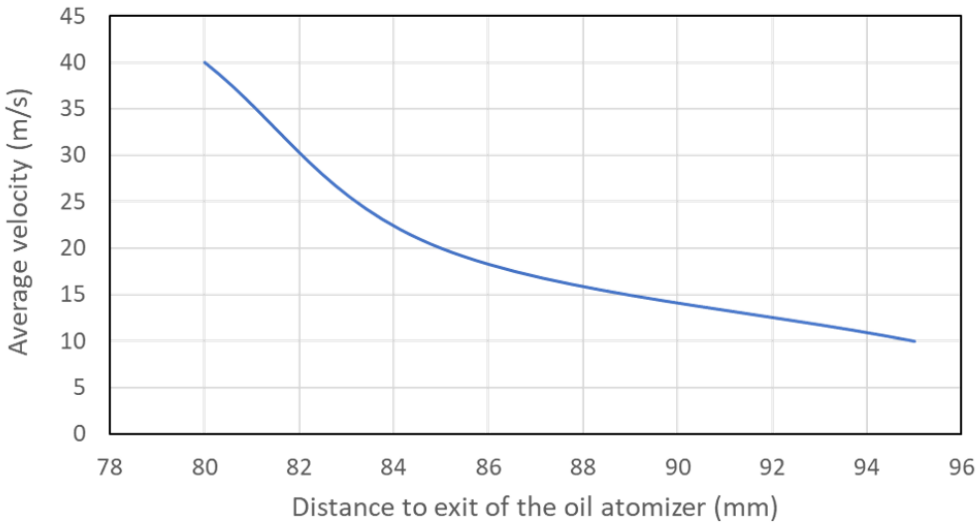

Figure 3.3: Average particle velocity profile near the substrate.

The experiments with the oil atomizer presented PIV as a reliable diagnostic method that makes it possible to characterize sub-micron particles' velocity and trajectory. Moreover, PIV was utilized to study the flow features like the stagnation zone and perturbation. The stagnation zone where the particles deflected as they get close to the substrate are visualized in Figure 3.2. The analytical solution of stagnation flow can be compared with the PIV measurement. Consider the steady flow of an inviscid and incompressible fluid near the stagnation point of the substrate, the continuity, and the momentum equation reduces to Laplace's and Bernoulli's equation, respectively [50].

$$\nabla^2\phi = \frac{\partial^2\phi}{\partial x^2} + \frac{\partial^2\phi}{\partial y^2} = 0 \tag{2}$$

$$\frac{d\phi}{dt} + \frac{p}{\rho} + \frac{1}{2}V^2 + gz = const \tag{3}$$

$$V = |\nabla\phi| \quad or \quad u = \frac{\partial\phi}{\partial x} \quad v = \frac{\partial\phi}{\partial y} \tag{4}$$

The velocity along the plate surface is achieved by solving equations 2, and 3. 2a is the height of the plate.

$$\frac{v}{U} = \frac{\frac{y}{a}}{(1-\frac{y^2}{x^2})^{\frac{1}{2}}} \tag{5}$$

The velocity distribution along the radial distance to the center of flow is provided in Figure 3.4 at about 2 mm away to the substrate. It has shown by red color in Figure 3.5 which illustrated the streamline for stagnation flow. The velocity distribution over the radial axis of the oil atomizer shows the flow velocity grows linearly near the tip. The PIV results and streamline by the analytical solution for normal flow to the substrate revealed that streamline that approach to substrate vicinity deflect up and over with high velocities and low pressure near the tips. It could be concluded that the developed PIV test set-up has been verified at room temperature to study the flow by tracking

the sub-micron particles at room temperature. PIV can be implemented to understand the complex phenomenon in SPS by the observation of the sub-micron particle velocity and direction in a plasma gas.

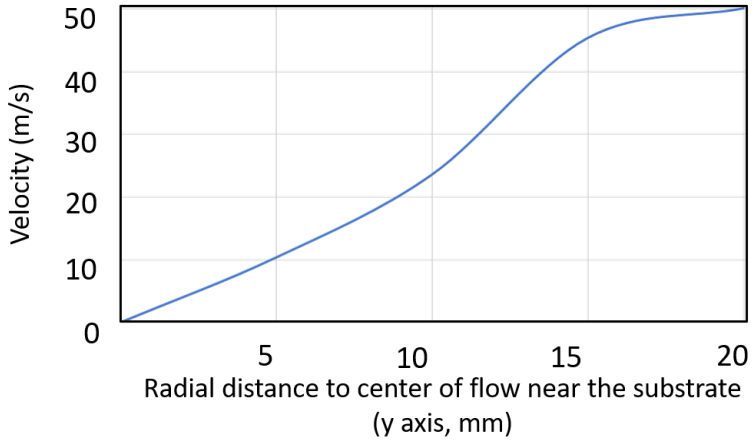

Figure 3.4: Velocity distribution along the radial distance of the centerline.

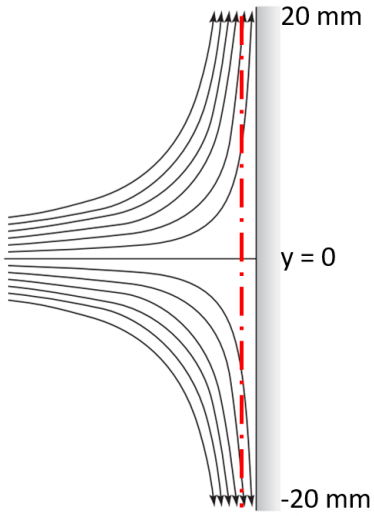

Figure 3.5: Streamline for stagnation flow over a flat substrate [50].

3.2 Plasma Flow Case

3.2.1 Visualization of Suspension Injection into the Plasma Plume

In this section, transport of suspension into the plasma plume is visualized to understand the complex phenomena such as suspension penetration, primary, and secondary atomization. The plasma breaks up the suspension to spray of droplets. Visualization of the water-based TiO_2 injection into the plasma plume is provided in Figure 3.6. The suspension is injected radially into the

plasma plume. The suspensions droplet that corresponded to the larger drops suspension dragged toward the downstream of the plasma plume, evaporated, and melted forming the final coating particles. These particles traveled mainly along the plasma plume that related to the small drops illustrated in the figure. This is an interesting observation that particles well penetrated in the crossflow, and the penetration effect close to the center of the torch axis identified. More precisely, particles have well penetration in the plasma for the conditions discussed in this study. This can practically be useful for SPS in which the suspension drops that penetrate efficiently into the plasma travel in the high temperature and high-velocity zone.

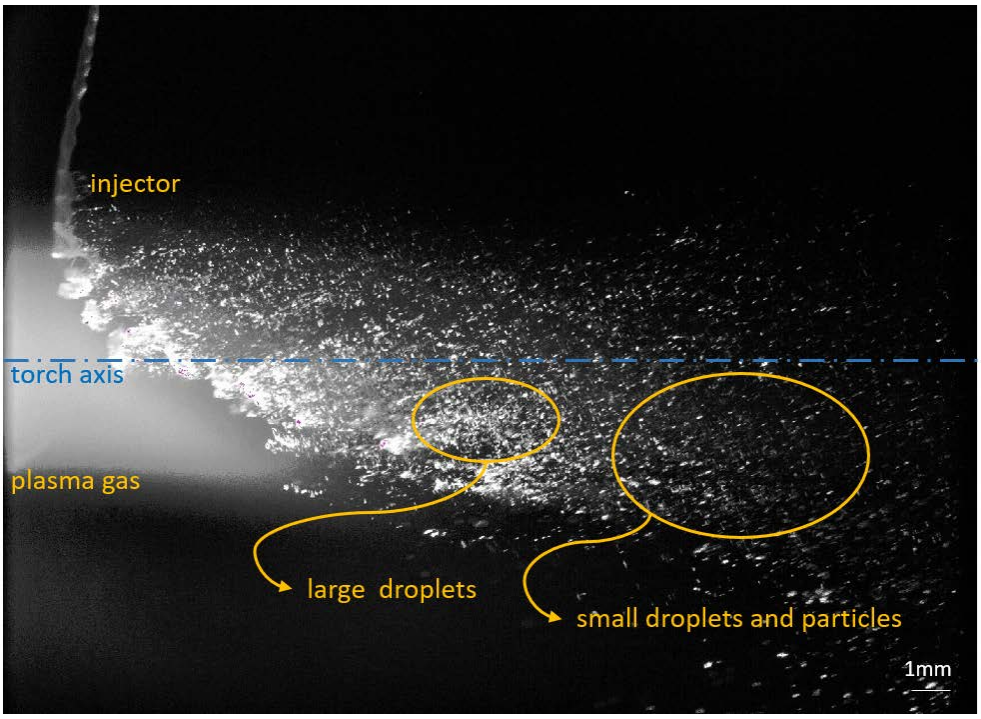

Figure 3.6: Flow visualization of TiO_2 aqueous suspension injection into the plasma plume.

Different size droplets were resulted from the atomization of suspension by plasma. The larger drop suspensions refer to droplets, a liquid phase composed of small particles in solid phases. In comparison, the small drops refer to the particles. Also, these fine particles can agglomerate during the process and create different size distributions. In the following section, the velocity field characterization of the TiO_2 water-based suspension with and without substrate inclusion was investigated using the developed PIV set-up at room temperature.

3.2.2 Free Jet

This section is dedicated to the investigation of suspension jet into a plasma cross flow. PIV measurements have been presented at two different windows of interest (centerline and 9 mm above the centerline). The velocity vector field at a standoff distance 50 mm along the centerline is shown in Figure 3.7.

Figure 3.7 displays the suspension injection into a free jet and in-flight particle trajectories that are traveling along with the plasma gas without any disturbance caused by the inclusion of a substrate. The result is corresponded to the green field of view shown in this figure. The velocity

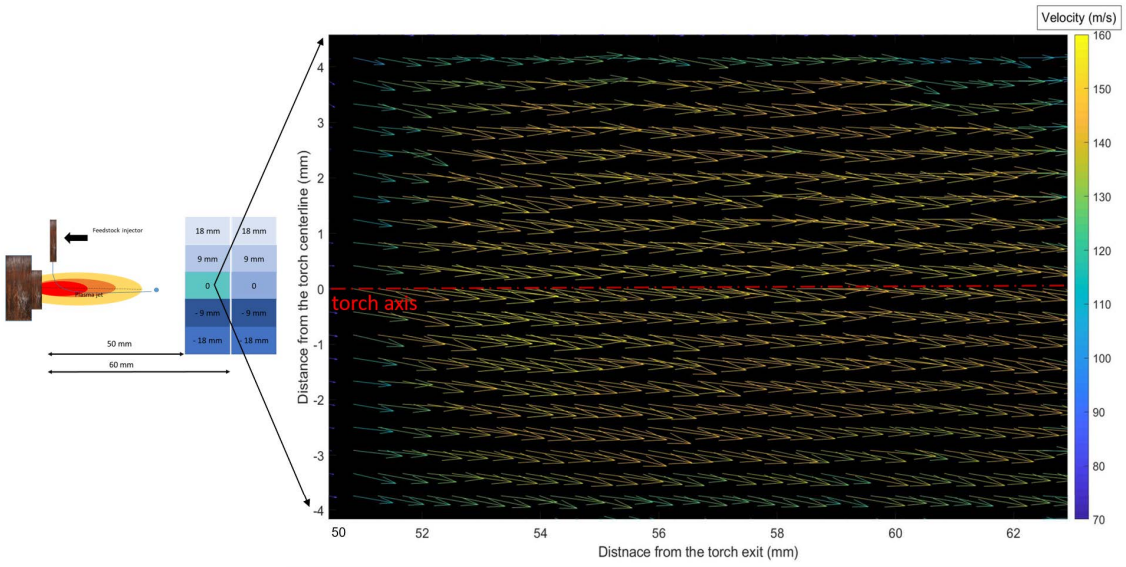

Figure 3.7: Velocity vector field in SPS process at a standoff distance of 50 mm.

distributions are obtained at the above and below the centerline. The maximum particle velocity is measured at the center of the plasma. The interesting area was chosen at the centreline therefore the averages of velocities are relatively remained the same for TiO_2 suspension drops and achieve to a high velocity in the range of $140 - 160$ m/s. This PIV measurement can be compared with a PIV measurement conducted by E. Aubignat et al. [40] that high-velocity zones are much more localized and closer to the torch axis for the water-based suspension. Figure 3.8 shows the velocity vector field captured at a standoff distance of 50 mm and 9 mm above the centerline as indicated by the green field of view.

When the particles are localized at a far distance to the plasma plume, the large droplet achieved. As observed in the image, these droplets are more affected by the plasma air disturbance, resulting in a lower velocity ($70 - 90$ m/s). However, the maximum velocity is measured 10 mm below the centerline. Figure 3.9 illustrates that area along the radial axis of the torch at standoff distance of 50 mm to the torch exit, is where suspension drops reached a high velocity. This area can be practically beneficial for the final characteristics of the coatings produced by SPS. While as the radial distance increased to the centerline, the shadowing effect might be expected due to the velocity deceleration.

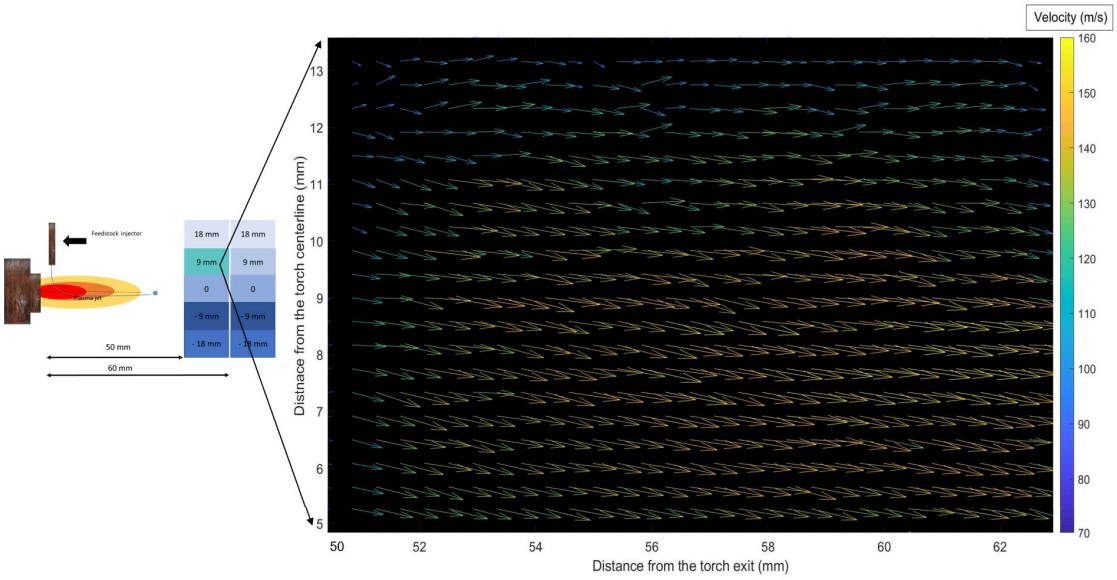

Figure 3.8: Velocity vector field in SPS process at 50 mm to the exit of the torch and 9 mm above the centerline.

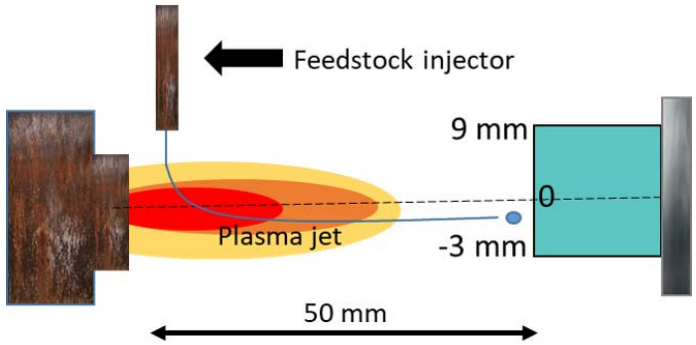

Figure 3.9: Schematic of the high velocity zone along the plasma jet estimated by PIV measurement in SPS at a standoff of 50 mm.

To further discuss this investigation, the effect of standoff distance on particles' characteristics in SPS is discussed by moving the interrogation window by 10 mm downstream the flow (D = 60 mm). Figure 3.10 and Figure 3.11 show the velocity vector field at D = 60 mm in the centerline and 9 mm above the centerline, respectively. The result is related to the green blocks, as shown in the images. By comparing PIV measurements at two standoff distances, suspension droplets decelerate and cool down by increasing the standoff distance. This is expected since the plasma axial velocity decreases along the centerline due to shear stress and increasing the drag force [28]. Subsequently, particles would impact the substrate with lower velocity by increasing the standoff distance. It can be concluded that particles at 50 mm standoff distance result in the denser coating by having higher velocity compared to the standoff distance of 60 mm to the torch exit. It was also reported in the relevant experimental tests that a uniform coating quality is obtained at around 50 mm standoff distances [51].

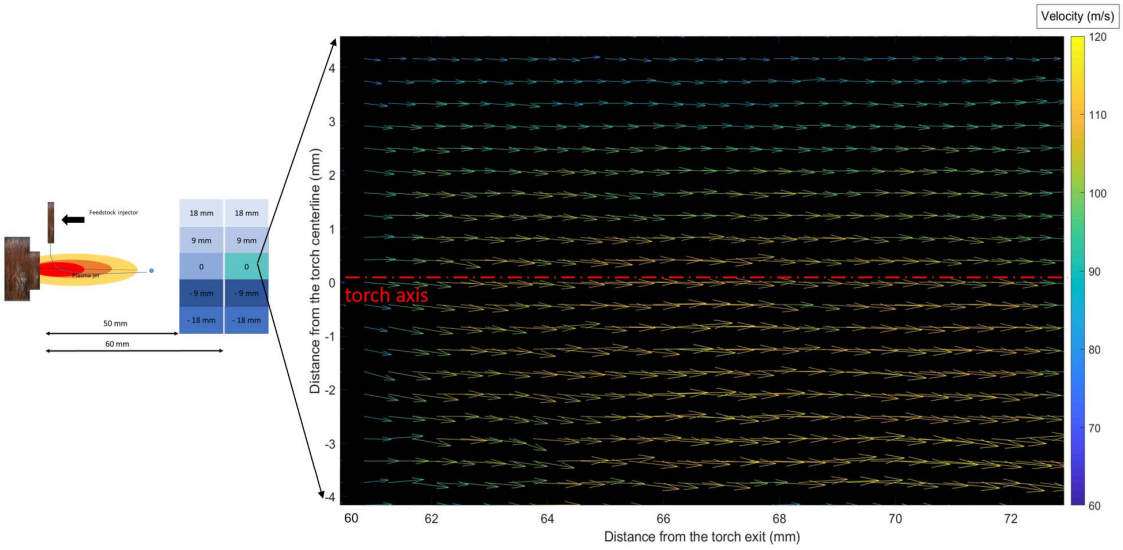

Figure 3.10: Velocity vector field in SPS process at a standoff of 60 mm.

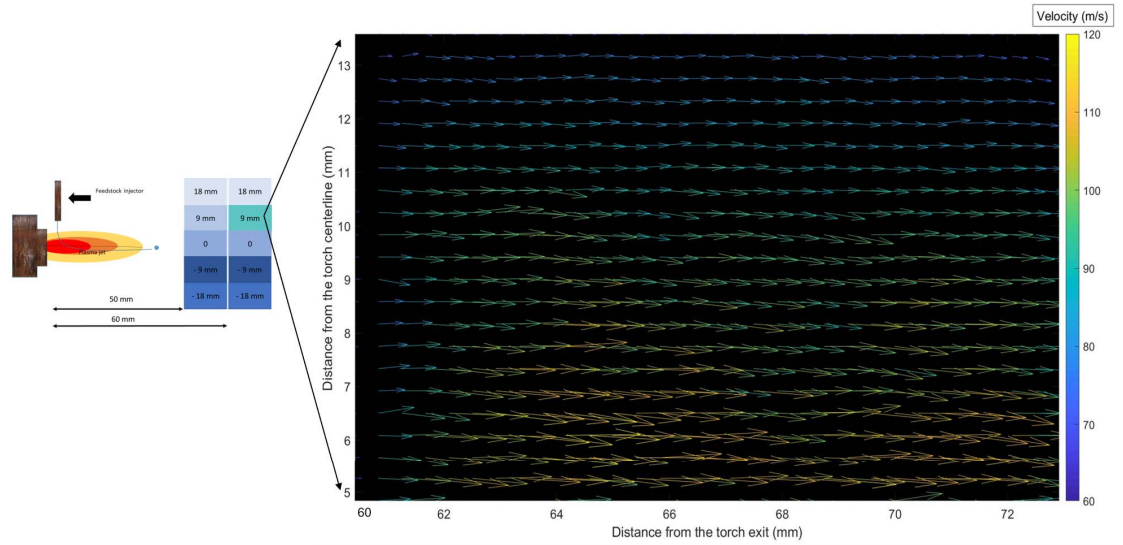

Figure 3.11: Velocity vector field in SPS process at 60 mm to the exit of the torch and 9 mm above the centerline.

Figure 3.12 (a) and (b) show the average velocity profile along the torch's radial axis, which corresponds to the determination of velocity vectors along the y-axis at spray distance 50 mm and 60 mm using various fields of view. In part a, the rate of velocities reduction was observed by increasing the distance. It also shows a maximum velocity at the center of the free plasma jet, which changes from $140 - 160$ m/s by increasing the standoff distance. According to b), the same trend was identified in the field of view 9 mm above the centerline. In comparison, the average velocities are decreased at this window since it was placed far from the torch axis, and suspensions drops reach a lower velocity compared to part a). The decreasing velocity indicates that those particles that travel along the periphery of plasma can be affected by the plasma turbulence and decelerate

to lower velocities ($60 - 80$ m/s). These droplets with relatively lower velocity correspond to the suspension drops that do not effectively penetrate the plasma plume. In a general view, coating particles with low velocity result in decreasing coating quality [28].

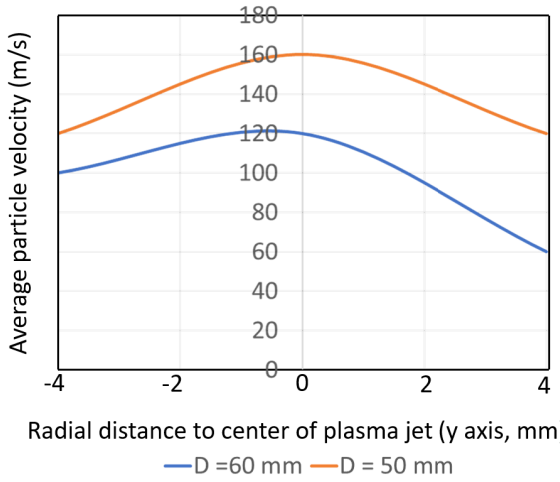

(a) Radial development of the average particle velocity magnitudes at the centerline

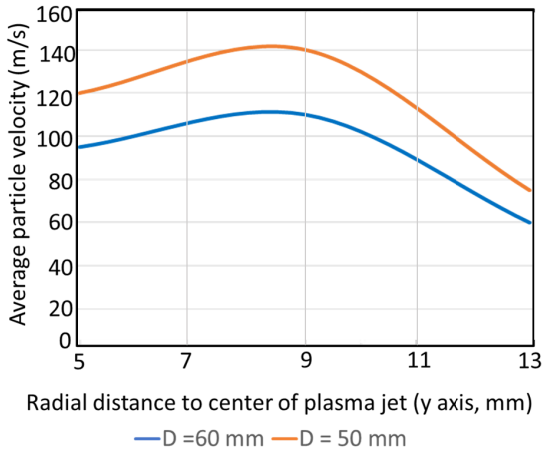

(b) Radial development of the average particle velocity magnitudes at 9 mm above the centerline

Figure 3.12: Radial development of the average particle velocity magnitudes at D $= 50$ mm and D $= 60$ mm from the torch exit, in the case of a free jet

In this study, it is shown that it is feasible to characterize particles' velocities and trajectories in the complex SPS process which includes challenges such as plasma radiation, limited access to test set-up due to high temperature operation, and the different size distribution of suspensions droplets in the process. More precisely, the presence of the droplets and particles provides more complexity compared to study at room temperature. For these reasons, ImageJ has been used to filter out the larger suspension droplets to investigate the velocity of small particles contributing to

the formation of SPS coatings. Moreover, the effect of eliminating large droplets on the average velocity magnitude was examined. Therefore, the larger droplets were removed using threshold and size analysis, by implementing a threshold that larger droplets are defined more than $10\ \mu$m. Figure 3.13 presents the velocity vector field at a standoff distance of 50 mm. According to the results, the average velocity is increased by $10 - 15$ m/s by removing the large droplets. It can be concluded that the PIV measurements estimated the combination of droplets and particles in the free jet. It is important to note that the PIV measurements in SPS can be used as a reference point to compare the particle velocities and trajectories in the presence of the substrate to observe how velocities and directions change as they get closer to the substrate.

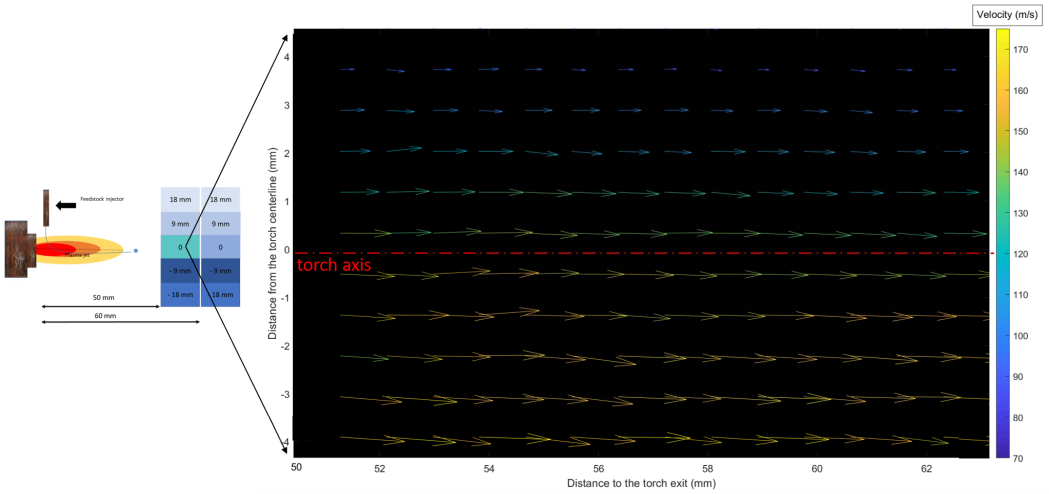

Figure 3.13: Velocity vector field in SPS process at 60 mm by setting threshold.

3.2.3 Stagnation Flow

The influence of the presence of a flat substrate on in-flight particles is shown in Figure 3.14. It shows that the trajectories of TiO_2 particles are affected by the change of the flow pattern caused by the presence of the substrate owing to their small Stokes number. These small particles also gain higher temperature and velocity compared to the larger ones. Moreover, as observed, the particles traveling along the centerline acquired a higher velocity (80 m/s) compared to those moving in the fringe of plasma gas. As they get closer to the substrate, the particles trajectories start to deviate more and the particle velocity decelerates. This points out the presence of the stagnation point generated by the substrate, which is examined in section 3.1.2 by atomizing DHES sub-micron particles at room temperature.

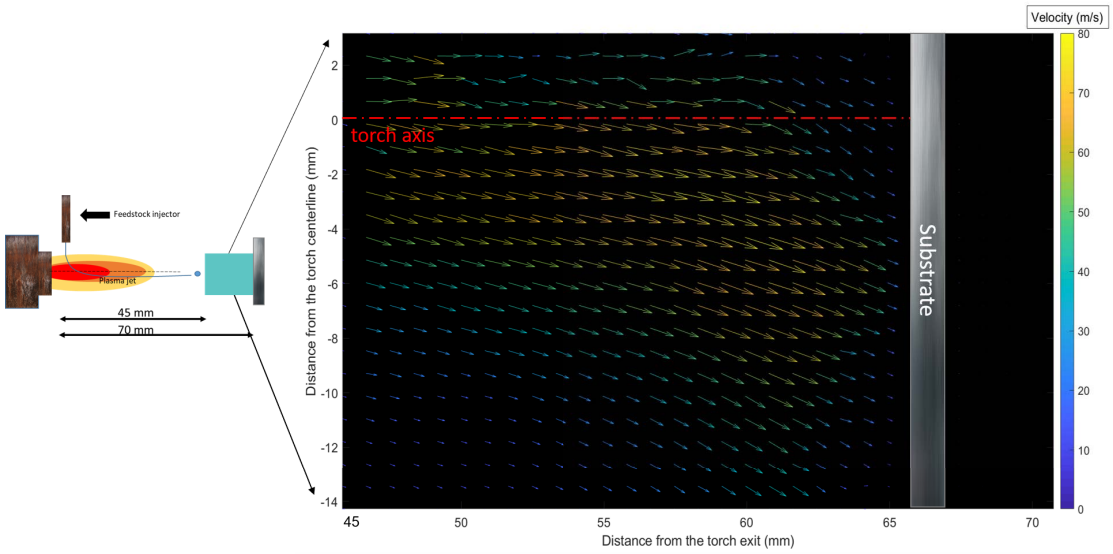

Figure 3.14: Velocity vector fields with TiO_2 aqueous suspension in the presence of a substrate.

In general view, when comparing the particles trajectories and velocity with and without the inclusion of a substrates, the average velocity drops between $80 - 40$ m/s at D $= 50$ mm and D $=$ 60 mm from the nozzle exit, respectively. Such velocity reduction in the presence of the substrate represents the effect of stagnation region, which disrupts the particle flow downstream and leads particles to a complete stop at the stagnation point which caused pressure increased in this region. The particle flow enters the wall jet region after turning and moving in the radial direction. It is also interesting to note that the effect of stagnation point and drag on particle trajectories is observed at 45 mm away to the nozzle exit. The deflection of particles are more pronounces compared to that of droplets. The PIV measurement could be compared to the numerical simulation obtained from Pourang et al. [28] studies. Figure 3.15 illustrated a cross-sectional view of the normal velocity of the particles impinging to the substrate at 40 and 60 mm standoff distances. The results at D $=$ 40 mm reveals that high temperature (molten) and high-velocity particles are traveling close to the centerline. By increasing the standoff distance, the particles cool down and decelerate at D $= 60$ mm. Moreover, the velocity of the particle surrounding the plume is lower than 100 m/s.

The PIV measurement are in good agreement with another study by Dolmair et al. [42]; the authors investigated the effect of inclusion of a flat substrate; they observed that the particle velocity value of 74 m/s at the center of the plasma jet. As a result, those particles deflecting by gas flow in the vicinity of the substrate, depositing on the sides of the asperities on the surface. This observation can be linked to the formation of columnar structure that was shown in Alebrahim et al. [1] with the same deposition parameters mentioned in this study. Figure 3.16 (a) and (b) displays SEM micrographs of TiO_2 deposited by SPS on stainless-steel substrate and a porous alumina substrate achieved from their work. In both cases with difference being the nature of the substrate, the bottom section of the coating is relatively homogeneous. Whereas, in homogeneous areas in consist of quite porous elongated zone were observed on the top section of coating. Such porous zone developed from shadow effect [15].

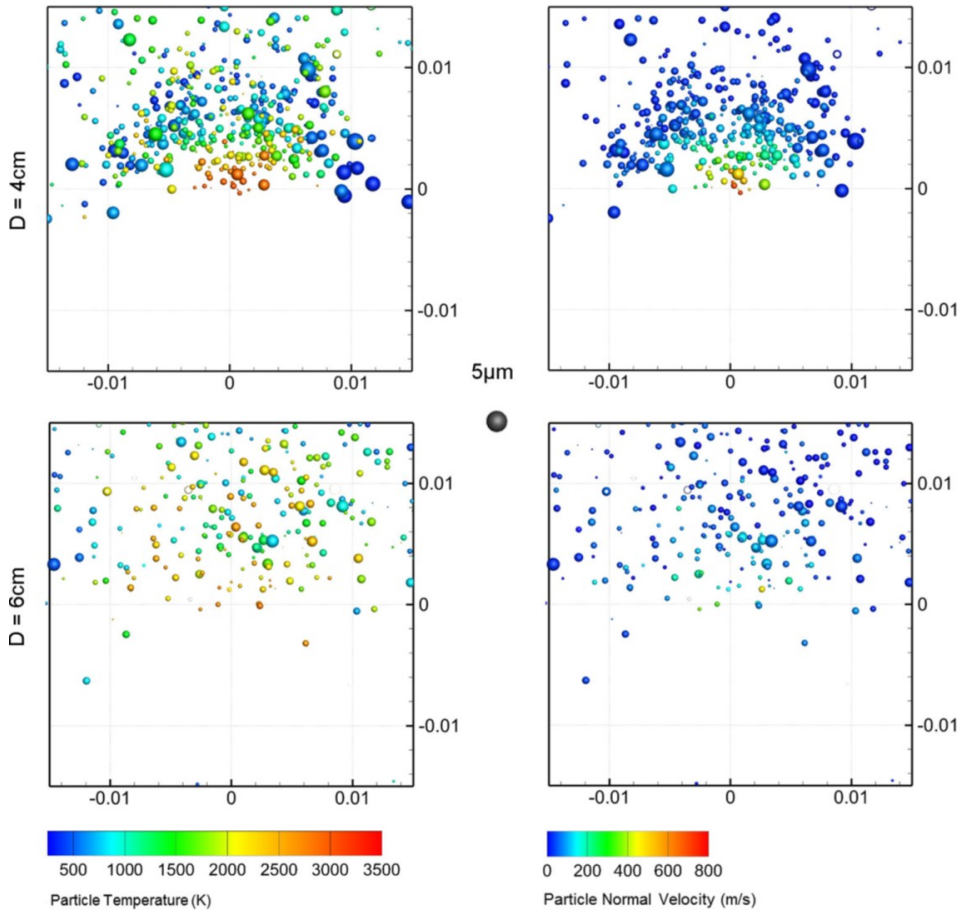

Figure 3.15: Landing location, particle velocity distributions on the substrate for standoff distances of 40 and 60 mm (dimensions are in meters) [28].

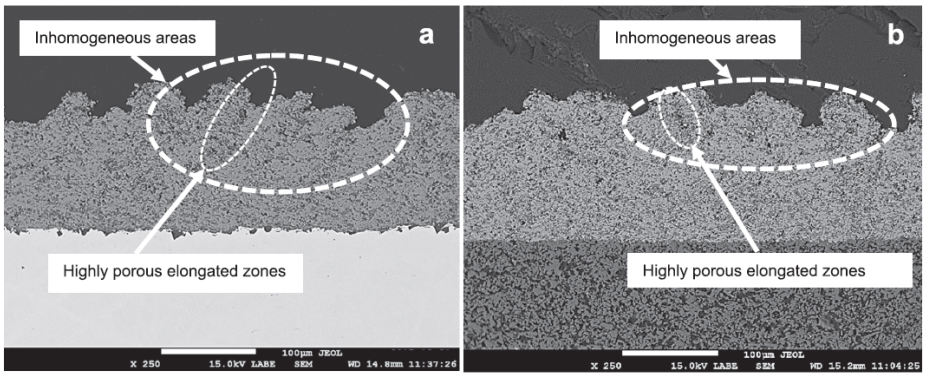

Figure 3.16: SEM micrographs of SPS TiO_2 coating; a) SPS-6 on stainless steel substrate, b) SPS-6 on a porous alumina substrate [1].

3.2.4 Comparison of the PIV Measurements and TES

In this section, TES is used to investigate particles' velocity at different points with the same condition as used for the PIV run. The particle velocity evaluated by TES and PIV techniques at 50

mm and 60 mm from the torch exit is provided in Figure 3.17. It should be noted that the velocity obtained by TES is around 210 to 250 m/s, which is twice the results achieved in this dissertation by PIV analysis. Although the trend for both cases are similar, the velocity values are not in the same range. The particle velocity detected with the PIV in free jet increased from 120 to 145 m/s. These results would agree with another research by Marchand et al. [39] Their results obtained with F4MB torch are around $100 - 210$ m/s, while the velocity measurement by TES is about 260-450 m/s. In order to confirm the significance of the PIV measurement, they concluded that the coating porosity was obtained corresponding to the velocity of particles achieved by PIV. According to these results, it could be concluded that PIV is well adapted to acquire the particles' velocity involved in the coating developed in SPS process. More precisely, it should be pointed out comparing TES and PIV results highlight the different diagnostic methods on particle velocity measurement. TES captured fine molten particles at high temperature and represented the higher velocity, while PIV measured the particle velocity of droplets containing liquids and are at room temperature. Regarding the explanation, two series of measurements are not in agreement.

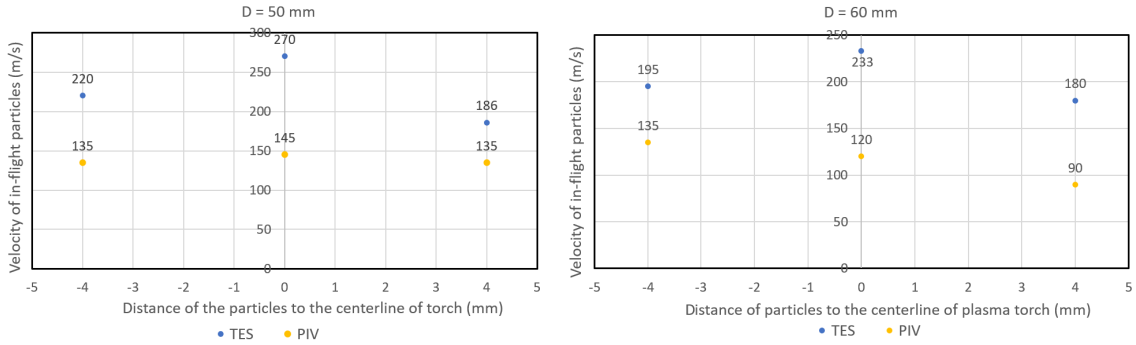

Figure 3.17: Particle velocity evaluated by TES and PIV techniques at 50 mm and 60 mm from the torch exit.

The schematic of particles and droplets are presented in Figure 3.18. The high velocity obtained by TES corresponded to those red particles with high temperatures. In the other research by Pourang et al. [4] the SPS process has been modeled and presented that the size distribution related to these high temperatures are below 2 μm at a 60 mm standoff distance from the torch. At the same time, the blue droplets in the schematic are captured with PIV. It can be concluded that for a better understanding and control of the SPS process, the complementary of two techniques is needed to diagnose the particles' velocity.

The experimental result obtained from Alebrahim et al. [1] were deposited with the parameters listed in Table 2.2 correlated with PIV result. SEM image of the cross-section TiO_2 deposited by SPS obtained from their work is provided in Figure 3.19. In a general view, the cross-sectional view shows the presence of large pores (A), un-melted particles (B) re-solidified particles (C), and fully melted zones (D). Fully melted section (D) related to the particle with having high velocity and high temperature traveling along the centerline. The finely porous zones corresponded to the un-melted particles. These particles travel within the verge of the plasma plume, which lead to lower velocity and thermal energy [34]. The small particles and agglomerating the feedstock particles were disclosed to high temperature resulted in sintering the fine particles without melting, in the verge of plasma plume. One exciting feature of this coating is that the existence of these un-melted particles creates unique porous structure which can be applicable for the filtration membrane application.

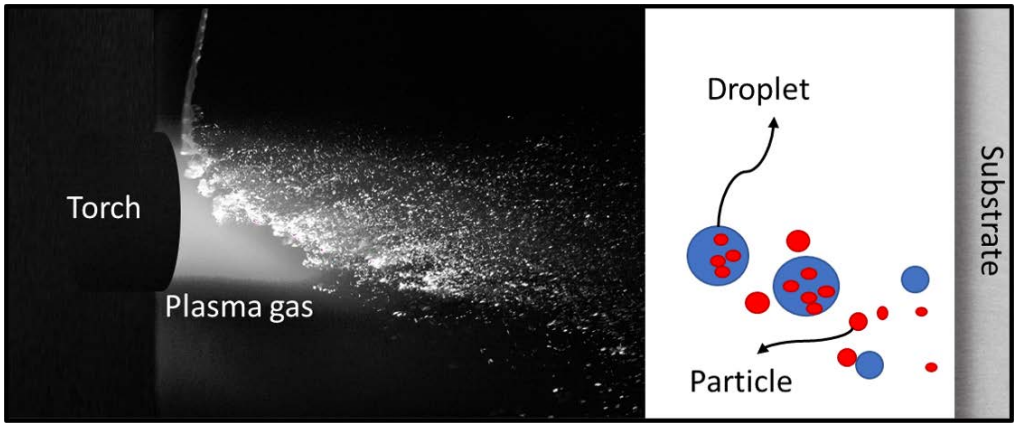

Figure 3.18: Schematic showing the droplets and particles involved in the suspension plasma spray process.

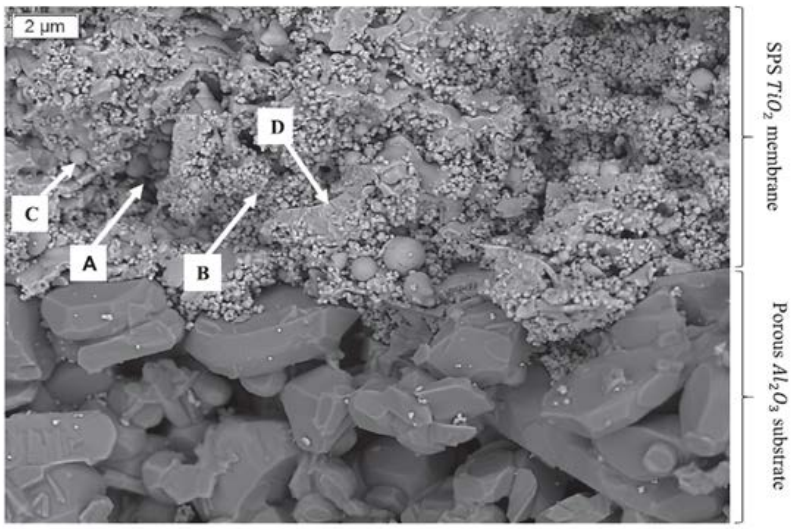

Figure 3.19: SEM micrograph of fractured cross- section of SPS TiO_2 membrane [1]

Chapter 4

Conclusion and Future Work

In this chapter

The conclusion of this study are presented. In addition, future work is discussed.

Experimental research was performed to a better understanding of SPS process to produce a coating with tailored structures. PIV analysis has been carried out to observe the sub-micron particles' velocity and trajectories in the free jet and the vicinity of a substrate.

4.1 Conclusion

This study is based on a non-intrusive diagnostic tool for studying the particles' behavior in the SPS process, which affects the coating microstructure. The experiments were performed in two steps: using a nebulizer at room temperature to simulate the SPS process and developing the test set up to avoid the harsh plasma environment to control the diagnostic process better. After getting acquainted and having validated the methodology with a similar process, the developed set-up was employed in the SPS process.

Since one of the aims of this work is to investigate the particles' characteristics in the free jet and stagnation flow conditions, different cases were studied to consider the inclusion of a substrate. In all these cases, the velocity field of the in-flight particles was studied. The results of these investigations demonstrated that particles tend to have higher average velocity close to the centerline compared to the particles travelling in the fringes of the plasma plume. More precisely, the fine particles that effectively penetrated the plasma plume reached higher velocities. The measured particle velocities also provide information on the injection quality, as the better the particles penetrate the plasma core, the higher their velocities will be. The PIV measurements carried out in this study confirmed the numerical and experimental results reported by other researchers [42, 28] on the effect of substrate and its shape on in-flight particle properties and trajectories.

In addition, it was also shown that, at room temperature and in the SPS process, the particle trajectories are deflected in front of a flat substrate, which is associated with a small Stokes number (< 1) of the sub-micron particles. The submicron particle flow persistently follows plasma jet streamlines and is even more sensitive to plasma turbulence near the substrate. Furthermore, these experimental results highlighted a stagnation zone near the substrate. The inclusion of a substrate disrupts the particle trajectories and reduced their velocity as compared to the free jet case. In SPS process, particles cannot reach velocities as high as the plasma gas velocity due to the low plasma gas density. These experimental results also highlighted that the particle's velocity measured by PIV are strongly influenced by the presence of relatively large suspension droplets, which agrees with the experimental observations by Alebrahim et al. [1]. The average particle velocity for these droplets is much lower than the plasma gas, which is in good agreement with a numerical study by Dalir et al. [52].

The complexity of the phenomena involved in the suspension plasma spray process, such as liquid jet atomization, particle agglomeration, and plasma radiation and reflection, and PIV set-up limitations, have made it difficult to fully monitor the particle behavior in the vicinity of a substrate. Moreover, a better characterization of submicron particle direction and velocity is still required to obtain a better understanding of particle trajectories for developing coatings with SPS. In this study, a key challenge is that particle velocity measured by PIV is affected by both droplets and particles. The separation of these two types of particles/droplets in the field of view is also challenging. Since the size distribution of particles was different in the SPS process due to particle agglomeration and evaporation. In general, this study highlighted that two complementary diagnostic tools could be used to better characterize and control the spray particle properties in the SPS process. As discussed above, PIV measurements provide information about the suspension droplets and relatively large particles, melted or not, while TES measurements are more sensitive to the small micro-sized

particles that are heated at high temperature. The results obtained by these two diagnostic techniques improved our knowledge of the droplet and particle velocities in the SPS process.

4.2 Future Works

Some future steps identified below can improve and strengthen this study.

- It should be pointed out that PIV measurements give information on particle velocities and trajectories: however, data on particle temperatures or their melting state are also beneficial to understand the phenomena occurring inside the plasma spray;
- Focusing on describing submicron particles at the impact on the flat substrate by using refined PIV set-up;
- Studying the effect of different substrate shapes on the behavior of the particles and coating microstructure;
- Investigating the particle velocity in axial suspension injection and to understand the coating microstructure;

Bibliography

[1] E. Alebrahim, F. Tarasi, M. S. Rahaman, A. Dolatabadi, and C. Moreau. Fabrication of titanium dioxide filtration membrane using suspension plasma spray process. *Surface and Coatings Technology*, 378:124927, 2019.

[2] N. Sharifi, M. Pugh, C. Moreau, and A. Dolatabadi. Developing hydrophobic and superhydrophobic TiO_2 coatings by plasma spraying. *Surface and Coatings Technology*, 289:29–36, 2016.

[3] J. R. Davis et al. *Handbook of Thermal Spray Technology*. ASM International, 2004.

[4] K. Pourang. Effect of substrate on in-flight particle characteristics in suspension plasma spraying. Master's thesis, Concordia University, 2015.

[5] P. L. Fauchais, J. VR Heberlein, and M. I Boulos. Wire arc spraying. In *Thermal Spray Fundamentals*. Springer, 2014.

[6] V. Burt, S. Lampman, A. Nolan, K. Marken, E. Marquard, J. H. Leyda, and B. Riley. ASM Handbook w. 2013.

[7] H. Khatibnezhad, F. Ambriz-Vargas, F. B. Ettouil, and C. Moreau. An investigation on the photocatalytic activity of sub-stoichiometric TiO_2-x coatings produced by suspension plasma spray. *Journal of the European Ceramic Society*, 2020.

[8] M. A. Dragan, P. Strutt, and R. Maric. Crystallization and microstructure of metastable water quenched nanostructured 8 mol% yttria-stabilized zirconia using the solution precursor plasma spray method. *Journal of Materials Science*, 49(8):3215–3224, 2014.

[9] M. Jadidi, M. Mousavi, S. Moghtadernejad, and A. Dolatabadi. A three-dimensional analysis of the suspension plasma spray impinging on a flat substrate. *Journal of Thermal Spray Technology*, 24(1-2):11–23, 2015.

[10] Y. Bai, Sh. J. Zhou, L. Shi, W. Ma, and C. W. Liu. Fabrication and characterization of suspension plasma-sprayed fluoridated hydroxyapatite coatings for biomedical applications. *Journal of Thermal Spray Technology*, 2(8):1322–1332, 2018.

[11] P. Fauchais, V. Rat, J. F. Coudert, R. Etchart-Salas, and G. Montavon. Operating parameters for suspension and solution Plasma-Spray coatings. *Surface and Coatings Technology*, 202(18):4309–431, 2008.

[12] D. Waldbillig and O. Kesler. Effect of suspension plasma spraying process parameters on ysz coating microstructure and permeability. *Surface and Coatings Technology*, 205(23-24):5483–5492, 2011.

[13] R. Vaßen, H. Kaßner, G. Mauer, and D. Stöver. Suspension plasma spraying: process characteristics and applications. *Journal of Thermal Spray Technology*, 19(1-2):219–225, 2010.

[14] O. Rezania. Anelastic behavior of suspension plasma sprayed ceramic coatings. Master's thesis, Concordia University, 2016.

[15] K. VanEvery, M. J. Krane, R. W. Trice, H. Wang, W. Porter, M. Besser, D. Sordelet, J. Ilavsky, and J. Almer. Column formation in suspension plasma-sprayed coatings and resultant thermal properties. *Journal of Thermal Spray Technology*, 20(4):81–828, 2011.

[16] J. O. Berghaus, S. Bouaricha, J. G. Legoux, and C. Moreau. Injection conditions and in-flight particle states in suspension plasma spraying of alumina and zirconia nano-ceramics. In *Proceedings of the International Thermal Spray Conference*. May, 2005.

[17] N. Curry. *Design of Thermal Barrier Coating Systems*. PhD thesis, University West, 2014.

[18] G. Schiller, R. H. Henne, M. Lang, R. Ruckdäschel, and S. Schaper. Development of vacuum plasma sprayed thin-film SOFC for reduced operating temperature. *Fuel Cells Bulletin*, 3(21):–12, 2000.

[19] W. Jung, J. O. Dereux, W. C. Chueh, Y. Hao, and S. M. Haile. High electrode activity of nanostructured, columnar ceria films for solid oxide fuel cells. *Energy & Environmental Science*, 5(9):8682–8689, 2012.

[20] S. Ghafouri Azar. Three-dimensional simulation of coating build-up in suspension plasma spray process. Master's thesis, Concordia University, 2018.

[21] G. Guignard, A. Mauer, R. Vaßen, and D. Stöver. Deposition and characteristics of submicrometer-structured thermal barrier coatings by suspension plasma spraying. *Journal of Thermal Spray Technology*, 21(3-4):416–424, 2012.

[22] L. Łatka. Thermal barrier coatings manufactured by suspension plasma spraying-a review. *Advances in Materials Science*, 18(3):95–11, 2018.

[23] B. Bernard, L. Bianchi, A. Malie, A. Joulia, and B. Remy. Columnar suspension plasma sprayed coating microstructural control for thermal barrier coating application. *Journal of the European Ceramic Society*, 36(4):1081–1089, 2016.

[24] B. Bernard, A. Quet, L. Bianchi, A. Joulia, A. Malié, V. Schick, and B. Rémy. Thermal insulation properties of YSZ coatings: suspension plasma spraying (SPS) versus electron beam physical vapor deposition (EB-PVD) and atmospheric plasma spraying (APS). *Surface and Coatings Technology*, 318:122–128, 2017.

[25] P. Fauchais, M. Vardelle, S. Goutier, and A. Vardelle. Key challenges and opportunities in suspension and solution Plasma Spraying. *Plasma Chemistry and Plasma Processing*, 35(3):511–525, 2015.

[26] F. Jabbari, M. Jadidi, R. Wuthrich, and A. Dolatabadi. A numerical study of suspension injection in plasma-spraying process. *Journal of Thermal Spray Technology*, 23(1-2):3–13, 2014.

[27] C.W. Kang, H.W. Ng, and S.C.M. Yu. Comparative study of plasma spray flow fields and particle behavior near to flat inclined substrates. *Plasma Chemistry and Plasma Processing*, 26(2):149–15, 2006.

[28] K. Pourang, C. Moreau, and A. Dolatabadi. Effect of substrate and its shape on in-flight particle characteristics in suspension plasma spraying. *Journal of Thermal Spray Technology*, 25(1-2):44–54, 2016.

[29] P. Sokołowski, S. Kozerski, L. Pawłowski, and A. Ambroziak. The key process parameters influencing formation of columnar microstructure in suspension plasma sprayed zirconia coatings. *Surface and Coatings Technology*, 260:97–106, 2014.

[30] R. C. Seshadri, G. Dwivedi, V. Viswanathan, and S. Sampath. Characterizing suspension plasma spray coating formation dynamics through curvature measurements. *Journal of Thermal Spray Technology*, 25(8):1666–1683, 2016.

[31] C. Moreau, P. Gougeon, M. Lamontagne, V. Lacasse, G. Vaudreuil, and P. Cielo. On-line control of the plasma spraying process by monitoring the temperature, velocity, and trajectory of in-flight particles. In *1994 Thermal spray industrial applications: Proceedings*. 1994.

[32] C. Moreau, J. F. Bisson, R. S. Lima, and B. R. Marple. Diagnostics for advanced materials processing by plasma spraying. *Pure and Applied Chemistry*, 77(2):443–462, 2005.

[33] W. Fan and Y. Bai. Review of suspension and solution precursor plasma sprayed thermal barrier coatings. *Ceramics International*, 42(13):14299–14312, 2016.

[34] P. Fauchais, M. Vardelle, S. Goutier, and A. Vardelle. Specific measurements of in-flight droplet and particle behavior and coating microstructure in suspension and solution Plasma Spraying. *Journal of Thermal Spray Technology*, 24(8):1498–1505, 2015.

[35] R. D. Keane and R. J. Adrian. Optimization of particle image velocimeters: Ii. multiple pulsed systems. *Measurement Science and Technology*, 2(10):963, 1991.

[36] Georg Mauer, Robert Vaßen, and Detlev Stöver. Comparison and applications of dpv-2000 and accuraspray-g3 diagnostic systems. *Journal of Thermal Spray Technology*, 16(3):414–424, 2007.

[37] A. Akbarnozari, S. Amiri, A. Dolatabadi, and C. Moreau. Analysis of scattering light from in-flight particles in suspension plasma spray for size measurement. *Journal of Thermal Spray Technology*, 28(4):678–689, 2019.

[38] J. Vattulainen, E. Hämäläinen, R. Hernberg, P. Vuoristo, and T. Mäntylä. Novel method for in-flight particle temperature and velocity measurements in plasma spraying using a single ccd camera. *Journal of Thermal Spray Technology*, 10(1):94–104, 2001.

[39] O. Marchand, L. Girardot, M.P. Planche, P. Bertrand, Y. Bailly, and G. Bertrand. An insight into suspension plasma spray: injection of the suspension and its interaction with the plasma flow. *Journal of Thermal Spray Technology*, 20(6):1310–1320, 2011.

[40] E. Aubignat, M.-P. Planche, D. Billieres, A. Allimant, L. Girardot, Y. Bailly, and G. Montavon. Optimization of the injection with a twin-fluid atomizer for suspension plasma spray process using three non-intrusive diagnostic tools. *Journal of Visualization*, 19(1):21–36, 2016.

[41] E. Aubignat, M.P. Planche, A. Allimant, D. Billières, L. Girardot, Y. Bailly, and G. Montavon. Effect of suspension characteristics on in-flight particle properties and coating microstructures achieved by suspension plasma spray. In *Journal of Physics: Conference Series*, volume 550, page 012019. IOP Publishing, 2014.

[42] A. Dolmaire, S. Goutier, A. Joulia, P.-M. Geffroy, M. Vardelle, and L. Bianchi. Experimental study of the impact of substrate shape and tilting on particle velocity in suspension plasma spraying. *Journal of Thermal Spray Technology*, 29(3):358–367, 2020.

[43] A. Melling. Tracer particles and seeding for particle image velocimetry. *Measurement Science and Technology*, 8(12):1406, 1997.

[44] R. D. Keane and R. J. Adrian. Theory of cross-correlation analysis of piv images. *Applied Scientific Research*, 49(3):191–215, 1992.

[45] L. Adrian, R. J. Adrian, and J. Westerweel. *Particle image velocimetry*. Number 30. Cambridge university press, 2011.

[46] M. Raffel, C.E. Willert, F. Scarano, C.J. Kähler, S.T. Wereley, and J. Kompenhans. *Particle image velocimetry: a practical guide*. Springer, 2018.

[47] J. Westerweel. Efficient detection of spurious vectors in particle image velocimetry data. *Experiments in Fluids*, 16(3-4):236–247, 1994.

[48] The standard in optical filters for life science. https://www.semrock.com/, May 2015.

[49] H. L. Qin, G. B. Gu, and S. Liu. Preparation of nitrogen-doped titania using sol–gel technique and its photocatalytic activity. *Materials Chemistry and Physics*, 112(2):346–352, 2008.

[50] Frank M White. *Fluid mechanics*. Tata McGraw-Hill Education, 1979.

[51] M. Aghasibeig, M. Mousavi, F. B. Ettouill, R. Wuthrich, A. Dolatabadi, and C. Moreau. Electro-catalytically active porous nickel-based electrode coatings formed by atmospheric and by suspension plasma spraying. In *International Thermal Spray (ITSC) Conference and Exposition*, pages 13–15, 2013.

[52] E. Dalir, A. Dolatabadi, and J. Mostaghimi. Modeling the effect of droplet shape and solid concentration on the suspension plasma spraying. *International Journal of Heat and Mass Transfer*, 161:120317, 2020.